Journal of Structural Geology 189 (2024) 105287

Contents lists available at ScienceDirect

Journal of Structural Geology

journal homepage: www.elsevier.com/locate/jsg

Lithological control and structural inheritance on faults growth in multilayer foreland sequences

Frank Thomas [a,*], Franz A. Livio [a], Norberto De Marchi [b], Raffaele Bitonte [c]

[a] Department of Science and High Technology Insubria University, Como (CO), Italy
[b] Energean Italy S.p.A, Piazza Sigmund Freud, 1, 20154, Milano (MI), Italy
[c] Formerly Energean Italy S.p.A, Piazza Sigmund Freud, 1, 20154, Milano (MI), Italy

ARTICLE INFO

Keywords:
Structural inheritance
Fault re-activation
Foreland deformation
Lithological controls
Cover-restricted faults
Foredeep-forebulge systems

ABSTRACT

Foreland sectors and foredeep-forebulge systems are affected, as the orogenic wedge migrates, by successive stages of stress states and tectonic deformation, resulting in the development of complex fault networks, even if characterized by limited deformation. The role played by structural inheritance and changes in stress field through time, in influencing the successive re-activations of fault segments, is still a topic to be thoroughly investigated. In this work, thanks to an extensive database made available by courtesy of Energean, we were able to investigate a foreland sector at the margin of the southern Apennines. By means of thickness analysis of the Neogene foredeep sequence and of displacement analysis along the fault network, we documented a shift from forebulge-related extension, in Zanclean, to a new tectonic phase, since Piacenzian, related to a strike slip stress field, possibly related to the activity of the Tremiti Fault Zone. We also characterized the geometry and connectivity of the cover-restricted faults, developing above propagating normal faults and observed a clear correlation between fault propagation tendency and lithological/mechanical layering within the cover units.

1. Introduction

The Apennines, of Italy, are a prime example of a recent orogenic wedge, where previously rifted margins have been later progressively incorporated into the orogenic system, in foreland sectors (Mazzoli, 2000; Shiner et al., 2004a,b; Butler and Mazzoli, 2006; Vai and Martini, 2013; Pace and Calamita, 2014; Bitonte et al., 2021). The dynamics influencing the foredeep and the peripheral bulge system have already been extensively investigated: as the wedge migrates toward the foreland, the latter experiences a first phase of far-field compressive tectonic stress (Ziegler et al., 1995a; Lacombe and Mouthereau, 2002; Butler and Mazzoli, 2006; Mouthereau and Lacombe, 2006; Ahmadhadi et al., 2007; Scisciani, 2009; Pace et al., 2015; Craddock et al., 2017; Scisciani and Esestime, 2017), then extension due to lithospheric forebulging (Turcotte and Schubert, 2002; Billi and Salvini, 2003; Quintà and Tavani, 2012) and, finally, the foreland can be involved in the outer thrusts of the chain and being incorporated into the wedge (Tavani et al., 2015a). On the other hand, additional research is needed to the understanding of the faults' growth mechanisms and of the characterization of the structural network that controls the foreland basin evolution, under such rapidly changing tectonic environment (Argnani and Frugoni, 1997; Quintà and Tavani, 2012; Tavani et al., 2015b; La Bruna et al., 2018; Agosta et al., 2023).

Particular effort should be posed in deciphering the role exerted by structural inheritance and by a lithologic control on the development of foreland structural networks, as has already been extensively documented in different rifting settings (Gawthorpe and Leeder, 2000; Butler et al., 2006; Tvedt et al., 2013; Phillips et al., 2016; Naliboff et al., 2017; Rotevatn et al., 2018; Tavani et al., 2021). In fact, in these settings the development of faults networks, affecting alternating sands and shales tend to compartmentalize fault deformation into a stack of contrasting mechanical layers and can inhibit a direct upward propagation of faults, promoting instead the development of mechanically restricted faults (Wilkins and Gross, 2002; Soliva and Benedicto, 2005; Tavani et al., 2006; Roche et al., 2012).

In this study, we investigate the lithological control on faults growth and propagation along a foreland sector of the Southern Apennines. We present a case study where the foreland sector is cut by sets of normal faults with different orientation and investigate the faults growth through the Plio-Quaternary, when the area shifted from forebulging to

* Corresponding author.
E-mail addresses: ftxxx@uninsubria.it (F. Thomas), franz.livio@uninsubria.it (F.A. Livio), ndemarchi@energean.com (N. De Marchi), raffaele.bitonte@gmail.com (R. Bitonte).

https://doi.org/10.1016/j.jsg.2024.105287
Received 10 April 2024; Received in revised form 16 September 2024; Accepted 5 November 2024
Available online 8 November 2024

transtensional tectonics. We record and disentangle successive episodes of faults growth (Lacombe et al., 2009) and re-activations (Scisciani, 2009), by means of along-strike and along-dip displacement profiles analysis (e.g., Soliva et al., 2006; Roche et al., 2012; Tvedt et al., 2013) compared to the lithology of the foredeep sequence, in order to investigate possible mechanical control on fault propagation and growth.

Finally, a comparison with the present-day stress field, derived from the inversion of selected moment tensor solutions, will be discussed. The findings from this study provide important insights on the factors controlling faults growth and propagation, linkage, and structural connectivity in foredeep basins, where faults are typically immature and highly segmented.

2. Geological and structural setting

The study area is located ahead of the northern sector of the Southern Apennines, where a foreland domain is close to being incorporated into the orogenic wedge (Fig. 1). It belongs to the Adriatic microplate, part of the North African continental margin (Anderson, 1987; Battaglia et al., 2004; Piccardi et al., 2011) and has been affected, during the Mesozoic to Eocene, by the deposition of a thick epicontinental carbonate sequence and that was later subducted under the Apennines during the Neogene (Malinverno and Ryan, 1986; Royden et al., 1987; Royden and Faccenna, 2018).

Since Late Triassic, the Adriatic plate has been affected by a long-lasting extensional tectonic phase (Winter and Tapponnier, 1991; Vlahović et al., 2005), possibly interrupted in the Early Cretaceous (Ziegler et al., 1995b) and ending up in the Eocene (Casero and Roure, 1994). Locally, the fragmentation of the continental lithosphere resulted in an articulated palaeogeography, characterized by shallow-water carbonate shelfs (e.g., the Apulian platform) surrounded by pelagic domains (e.g., the Umbria-Marche and Lagonegro-Molise domain; Merlini and Mostardini, 1986; Patacca and Scandone, 2007; Patacca et al., 2008; Cosentino et al., 2010). The Late Cretaceous-Eocene period was marked by an abortive rift that ultimately ended up with the dismembering of the Apulian platform (Vitale and Ciarcia, 2013).

Later, the Adriatic margin has been progressively involved into the orogenic wedge of the Apennines, a fold and thrust belt formed since the Neogene within the geodynamic framework of Africa-Eurasia plate convergence (Doglioni, 1991; Patacca et al., 2008; Malusà et al., 2016; Piana Agostinetti and Faccenna, 2018; Fellin et al., 2021). This chain has been alternatively interpreted as: i) characterized by the stacking of a thin-skinned thrust system, with imbrications of sedimentary units detached above a substantially undeformed crystalline basement (Bally, 1986; Merlini and Mostardini, 1986; Hill and Hayward, 1988; Calamita et al., 1991; Cavinato et al., 1994; Ghisetti and Vezzani, 1997; Scrocca et al., 2005; Patacca and Scandone, 2007) or, ii) by deeply rooted thick skinned tectonics, partly re-activating inherited normal faults (Mazzoli, 2000; Shiner et al., 2004a,b; Scisciani and Montefalcone, 2006; Scisciani, 2009; Pace and Calamita, 2014), possibly coexisting (Butler and Mazzoli, 2006; Barchi and Tavarnelli, 2022). The eastward migration of the chain is dated back to the late Cenozoic due to the eastward and north-eastward flexural retreat of the Adriatic (foreland) lithosphere plate boundary (Patacca and Scandone, 1989).

In the Adriatic foreland, wedge-shaped Pliocene–Quaternary syn-orogenic sediments lie on top of the Messinian evaporites, unconformably lying on top of Mesozoic-Cenozoic carbonates and separated by a major regional erosive surface (i.e., the Messinian unconformity). Below this erosive surface, carbonates of the Adria plate are locally consisting of a Jurassic to Miocene sequence, mainly made up of limestones, deposited as carbonate shelf platforms and ramp sequences separated by unconformities (e.g., Ricchetti et al., 1988; Bosellini et al., 1999; Patacca et al., 2008; Cosentino et al., 2010; Santantonio et al., 2013) and recording some post-Cretaceous episodes of subaerial exposure (e.g., Mindszenty et al., 1995).

The stacking of the tectonic units in the Apennines followed an eastward migration of the thrust systems, with the development ahead of the thrust front of foredeep wedges filled by flysch -like sequences (Patacca and Scandone, 1989; Coward et al., 1999; Patacca et al., 2004; Critelli et al., 2011, among others) and a more external peripheral bulge system. Sabbatino et al. (2021) tracked the forebulge migration of the Central-Southern Apennines during the last 25 My, estimating a constant migration velocity of ca. 15 mm/yr.

The differential evolution and structural architecture of the Apennines, from north to south, resulted in the differentiation of the chain within the Northern, Central and Southern Apennines, with the front of the Northern Apennines extending far in the middle Adriatic whereas the external front of the Southern Apennines is markedly recessed. Some Authors (e.g., Argnani and Frugoni, 1997) interpret the recess between the Northern and Southern Apennines as a lateral ramp, due to the presence of the relatively rigid block of the Apulian Platform, inhibiting the propagation of the thrusts in the southern sector.

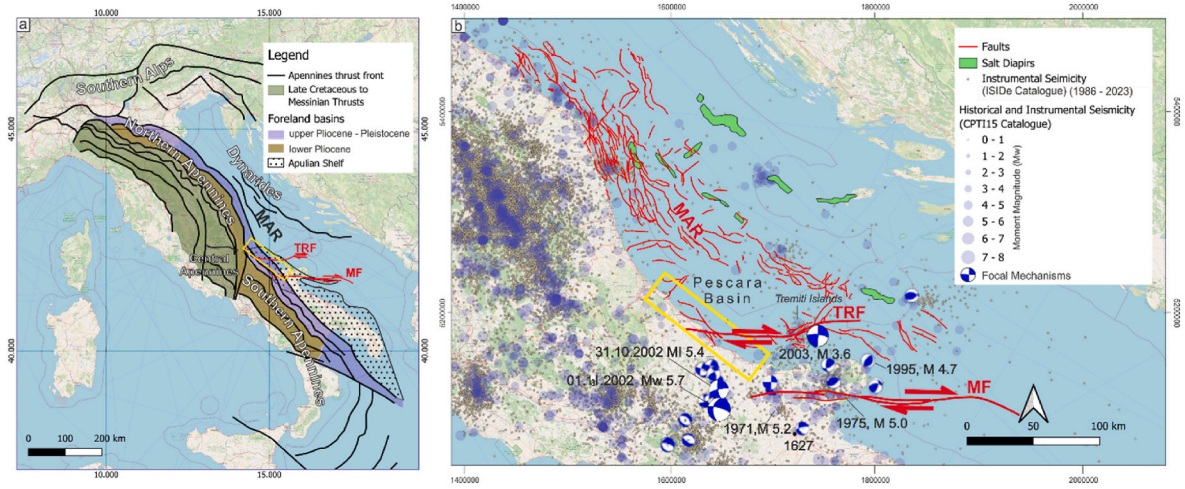

Fig. 1. regional geological and seismotectonic setting; the location of the study area (approximate, due to confidentiality of the dataset) is indicated with a yellow box: a) geological sketch of the Apennines (modified after Scrocca, 2006; Casero and Bigi, 2013) including the age and location of the foreland basins; b) seismotectonic setting of the study area: for historical and instrumental seismicity (ISIDe Working Group, 2007; Rovida et al., 2016); faults after Casero and Bigi (2013). Codes: MAR, Middle Adriatic Ridge; MF, Mattinata Fault; TRF, Tremiti Fault Zone. The Pescara basin bounded by the Tremiti Fault Zone borders the study area (modified after Casero and Bigi, 2013; Scrocca, 2006; Rovida et al., 2019; Di Bucci and Mazzoli, 2003; Di Bucci et al., 2006). (For interpretation of the references to colour in this figure legend, the reader is referred to the Web version of this article.)

Alternatively, following Scrocca (2006), the Tremiti Fault Zone is interpreted as the surface expression of a lithospheric tear within the subducting tear, below the Apennines. A differential speed in the retreat of the lower plate has been resulting in i) the uneven propagation of the Apennines thrust front (Fig. 1a); ii) the differential subsidence between the northern and southern sectors and iii) in the development of a lithospheric shear with dextral kinematics (Scrocca, 2006). This deeply rooted right-lateral shear zone is imaged by the CROP M13 deep seismic reflection profile (Finetti and Del Ben, 2005), which show a deeply rooted positive flower structure, close to the normal fault that bound the Apulian platform, to the east. Scisciani and Calamita (2009) highlight a possible positive inversion of an older and rift-related normal fault along the positive flower, supposing a detachment at the base of the upper crust instead. In any case, they confirm the presence of a structure related to wrench tectonics and focused in an area, the Central Adriatic Sea, that previously experienced extensional tectonics, and resulting in a weaker crust that later accommodated the differential movements among rigid blocks within the Adriatic plate.

The study area is located along the western margin of the Pescara basin (Fig. 1b), a sub-basin of the Adriatic Sea, closed between the front of the southern Apennines, to the southwest, and the fold and thrust belt of the Middle Adriatic Ridge (MAR), to the northeast. This latter is a NW-SE striking fold and thrust whose external front is touching the most external structures of the Dynarides (Finetti, 1982; Argnani and Gamberi, 1995; Argnani and Frugoni, 1997). Some Authors have highlighted a deep rooting for these structures that indeed are apparently cutting through the basement (e.g., Finetti and Del Ben, 2005a,b; Scisciani and Esestime, 2017; Pace et al., 2015; Carboni et al., 2024). Some of these structures, especially close the basin depocenter, in the most external fronts, show evidence of salt tectonics, diapirism and inversion tectonics (Pace et al., 2015). The MAR has been interpreted i) as being part of the accretionary wedge of the Apennines (Scrocca, 2006) or ii) as being the result of the far field stress transmission in the foreland, from a strongly coupled upper plate (Scisciani and Calamita, 2009).

During the Neogene, the study area has been involved into the flexure of the Apennines forebulge and accommodated the outer-arc extension through the movement of shallow rooted normal faults. Most of these faults ceased their activity during the Early Pliocene, but some sets of normal faults, characterized by a NW-SE strike, were later re-activated during a Late Pliocene tectonic phase, showcasing a normal dip slip component of slip.

The seismotectonic setting, as highlighted by historical and instrumental seismicity (Rovida et al., 2016), is characterized by relatively rare seismic events (Boschi et al., 2000;Guidoboni et al., 2019; Scrocca, 2006; Scisciani and Calamita, 2009, Fig. 1b), concentrated within a depth range of approximately 11–20 km.

The Oct. 31, 2002, Molise earthquake (Mw 6.0 and epicentral intensity VIII-IX MCS; Fig. 1b), was attributed to the strike-slip Mattinata Fault, consistently with the right-lateral focal mechanism solution (Di Luccio et al., 2005). Considering that the buried Apulia Platform is ca. 6 km thick, and its top lies at ca. 3 km of depth (e.g., Merlini and Mostardini, 1986); this implies that the seismogenic structures of the 2002 Molise earthquakes are located essentially within the basement of the Apulia Platform (Di Bucci et al., 2006).

The presence of this right-lateral slip component in the seismogenic source is consistent with findings from previous investigations related to the earthquakes of June 19, 1975, and July 24, 2003 (Anzidei et al., 1997; Ferranti and Oldow, 2005). Notably, this latter event exhibits a consistent alignment with the 2002 one and its focal mechanisms, even though surface faulting was not observed, in this case.

Most important historic seismic events in the area, such as the 1627 Gargano earthquake (Me = 6.8; Rovida et al., 2019), further underscore the connection to the Mattinata Fault (Di Bucci and Mazzoli, 2003; Di Bucci et al., 2006).

2.1. Stratigraphy

The study area is located along the margin of the Apulian carbonate shelf, which is bounded and locally dissected by Mesozoic normal faults (Fig. 2) active during successive pulses of extension, with a latest phase dated back at Aptian-Santonian (Santantonio et al., 2013). The Apulian carbonate platform passes, eastward, to the deep marine sequences of the Mesozoic Adriatic Basin. This transition is characterized by a shift from shelf platform carbonates to ramp successions. The youngest units of the Apulian platform are Miocene in age and are constituted by Messinian anhydrites and microcrystalline white limestone. A regional erosive surface the Messinian Unconformity marks the top of the platform when the platform carbonates are unconformably overlaid by Pliocene units. Overlying the Apulian carbonate platform is a Neogene clastic wedge, mainly made up of fine-grained deposits alternating with beds of sands.

In this study, we analysed 11 well logs to evaluate fault-related displacement across seven key stratigraphic horizons, spanning from the Messinian to the present day (Fig. 3), with the oldest one corresponding to the Messian Unconformity, three horizons within the Zanclean interval and three further horizons selected within the Piacenzian. The thickness ranges from 5 to 20 m; however, due to confidentiality agreements, the exact depths and thicknesses are not disclosed.

Based on the well reports, the Upper Miocene (Messinian) interval, when present, is predominantly made of massive anhydrite deposits, varying in colour from white to beige, and brecciated microcrystalline limestones.

The Zanclean interval, is predominantly composed of marly clay and clay interbedded with thin layers of fine to medium-grained sandstone and occasional limestone beds. The sandstone layers, though present, are relatively thin and suggest episodic deposition in a predominantly shale-rich low energy environment. Inclusions of bioclastic limestone are also observed, which may indicate brief periods of reduced clastic input. Additionally, the shale layers show intercalations of clay-carbonate cement and contain traces of pyrite, glauconite, and chlorite, with scattered occurrences of microfauna, particularly foraminifera.

The Piacenzian interval is characterized by alternating layers of sandy deposits and marly clays, indicative of a dynamic marine environment with varying energy conditions and sedimentation rates. The sandstones within this interval are fine to medium-grained, often interbedded with greyish-beige marly clays. These sandstone layers are decimetre-sized, well-sorted, and primarily composed of quartz, suggesting deposition in a higher-energy environment compared to the underlying Zanclean. In contrast, the marly clays represent periods of lower energy deposition, where finer sediments could settle, often alongside carbonate accumulation, as indicated by the presence of limestone beds within the marls.

A significant feature of the Piacenzian is a conglomerate layer found between the Piacenzian 2 and Piacenzian 3 horizons (Fig. 3). This layer points to a higher energy depositional environment, potentially linked to changes in sediment supply or increased proximity to a dynamic sediment source, such as during a storm or shift in sea levels. Throughout this interval, fossil content, particularly foraminifera, is abundant, especially within the marly clays, highlighting an active marine environment with varying depositional conditions. The presence of pyrite and glauconite within the sandy layers further suggests diagenetic processes under reducing conditions, which would be typical in environments with intermittent oxygen availability.

The Piacenzian depositional environment can be interpreted as a moderate to high-energy marine setting, likely on the continental shelf, where shifting sea levels and sediment supply played a crucial role in the alternating deposition of sands, clays, and conglomerates. The transition between sandy and marly layers, along with the presence of a conglomerate, marks the Piacenzian as a dynamic period with varying energy conditions, clearly defined by its lithological boundaries in the

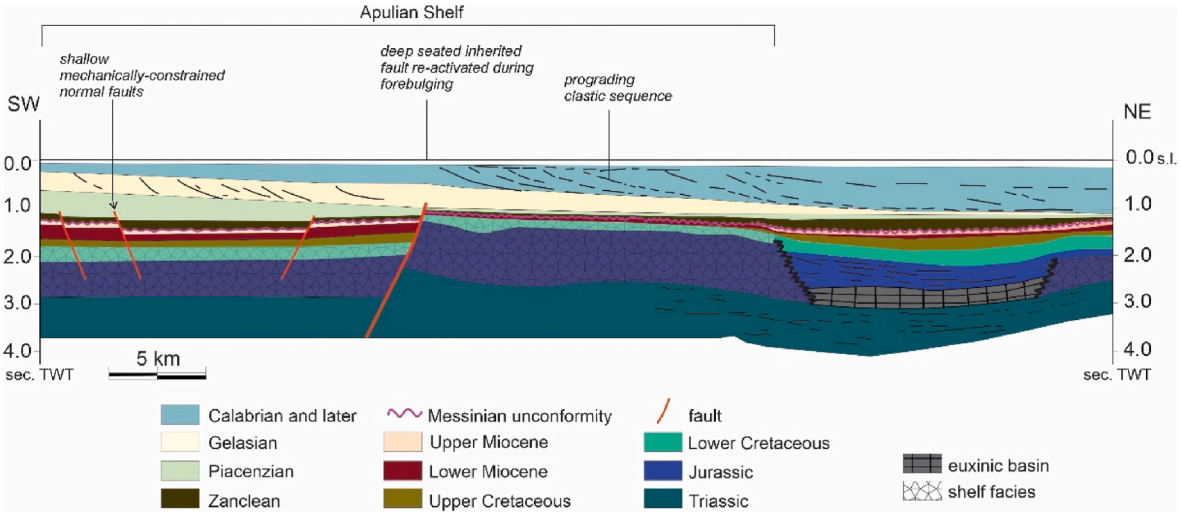

Fig. 2. a schematic geological cross-section across the study area (modified after Casero and Bigi, 2013): note the presence of both deep-seated normal faults, inherited from previous tectonic phases, and of shallow normal faults, mechanically constrained within the Apulian platform.

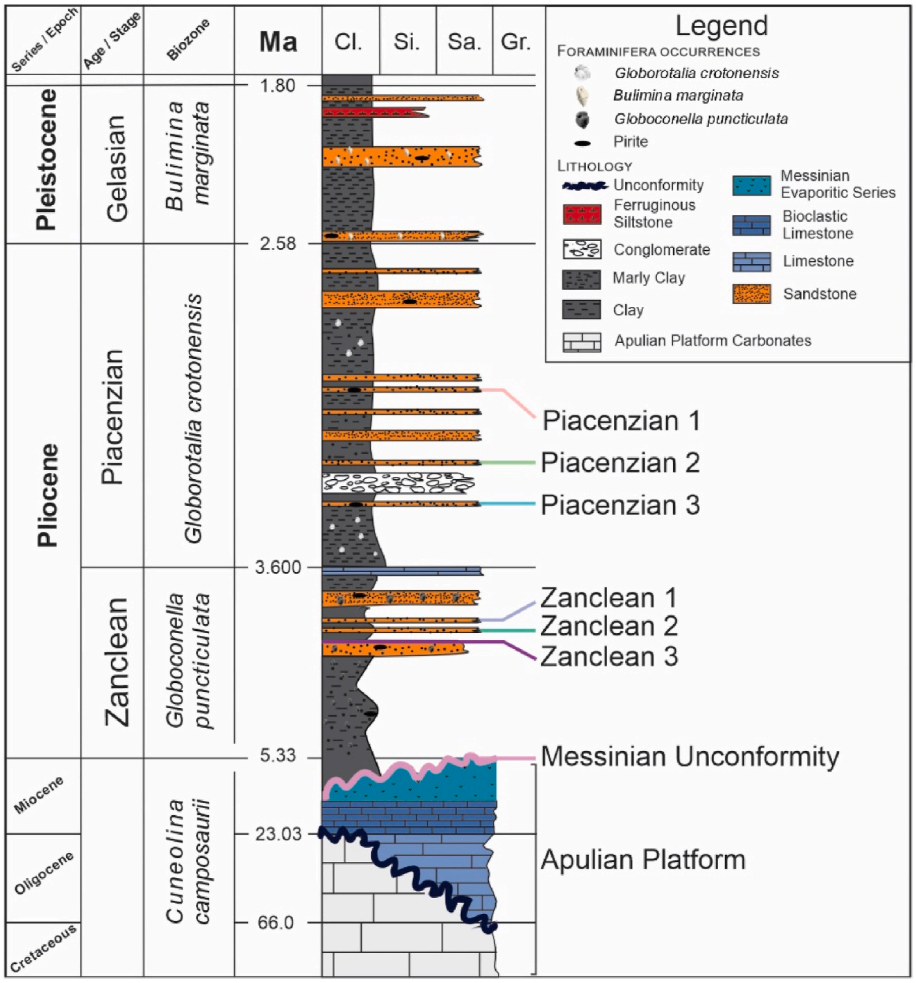

Fig. 3. Composite Stratigraphy of the study area and picked horizons, interpreted from well logs.

well logs.

Finally, the Gelasian interval, is characterized by alternating sequences of grey plastic calcareous clays interbedded with fine to medium-grained sands. These sands typically exhibit angular to sub-angular grains, indicative of deposition in a moderately energetic environment, likely influenced by fluctuations in sediment supply and water energy. The presence of clay-carbonate cement within the sandy layers suggests diagenetic processes that further solidified the sediments post-deposition.

The interval also includes layers of ferruginous siltstone, with

colours ranging from brown to reddish hues. This ferruginous nature indicates oxidation processes during or after deposition. Additionally, traces of pyrite, lignite, and mica are found throughout the interval, reflecting a depositional environment with varying redox conditions.

Within this section, microfauna is locally abundant, particularly foraminifera, which are more concentrated in the calcareous clay layers. This suggests a marine setting with episodic changes in environmental conditions, such as water depth and sediment influx.

The subdivision of the sequence into the Zanclean, Piacentian, and Gelasian stage was determined based on detailed micropaleontological reports from core samples. These reports allowed for precise biostratigraphic classification, ensuring well-defined boundaries between the intervals. The corresponding biozones, such as *Globoconella puncticulata* for the Zanclean, *Globorotalia crotonensis* for the Piacentian, and *Bulimina marginata* for the Gelasian, have been added to Fig. 3, which illustrates the subdivisions for the Zanclean (1, 2, 3), Piacentian (1, 2, 3), and Gelasian stages.

Additionally, insights from detailed well log data contributed to understanding the lithological composition and depositional processes of each stratigraphic interval.

3. Materials and methods

The precise location of the site remains undisclosed, due to the confidentiality of the data. The study includes 41 industrial seismic reflection lines with an average spacing of 500 m and 10 wells reaching a depth of approximately 2 km. The seismic data were acquired during multiple surveys, including a 2D seismic survey conducted in 1997 and reprocessed seismic lines from 1976 to 1982. These datasets were combined and post-processed to enhance the resolution of subsurface features. The 1997 survey comprised 2D lines with a shot point interval of 30 m, 120 channels, and 24 groups, covering approximately 47 km. Additionally, older seismic lines were reprocessed and merged using post-stack techniques to correlate with shallow water data from the adjacent concession. The seismic data underwent several processing steps to enhance data quality and improve geological interpretation. These steps included resampling and geometry assignment; application of field statics and residual statics corrections; deconvolution and low-cut filtering; surface wave noise attenuation and geometrical spreading compensation; frequency filtering and time-variant filtering (TVF).

Both post-stack migration and time migration were applied to improve the accuracy of structural imaging. Additionally, Amplitude Versus Offset (AVO) analysis was conducted to identify amplitude anomalies. The vertical resolution of the dataset is primarily constrained by the 4 msec sample interval, though additional information on the dominant frequency of the seismic wavelet is necessary for precise calculation. Horizontal resolution is determined by the 30 m shot point interval, and the survey achieved approximately 60% coverage of the subsurface target areas.

The well logs include gamma ray, sonic log, delta T, density logs, neutron porosity, resistivity log and spontaneous potential along with other geological logs and reports (composite log, velocity log, micropaleontological and palynological reports) that were used for stratigraphic correlations among wells, and to calibrate chronostratigraphically the stratigraphic intervals thanks to micropaleontological reports made available by Energean.

In cases where direct chronostratigraphic constraints were unavailable, intermediate horizons situated between two dated horizons were assigned approximate ages through the application of back-calculation techniques. This approach involved estimating the likely age of the intermediate horizons by assuming a linear age-depth relationship between known dated intervals. By employing this methodology, reasonable chronological estimates were established for the intermediate horizons, allowing for a more comprehensive understanding of the stratigraphic sequence. The stratigraphic intervals have been defined based on lithology, depositional environment, and stratigraphic relationship with major erosive surfaces and/or unconformities.

Building on this, we proceeded with seismic interpretation of key horizons (Fig. 3) and faults in the area.

The interpretation of the seismic data predominantly relied on the use of TWT (Two-Way-Travel Time) sections; interpreted horizons and faults have been later depth-converted for checking the well ties. Time-to-depth conversion has been performed by means of the velocity model developed by Energean and based on well velocities.

Here, we cannot disclose the depth of the analysed units nor their thickness, due to confidentiality requested by the owner of the dataset; thus, we will show the results in time domain (TWT). Nonetheless, considering that the average interval speed for the Plio-Pleistocene in the Adriatic foredeep ranges between 2000 and 2200 m/Sec (e.g., Mancinelli and Scisciani, 2020), when comparing the depths derived from well logs with the corresponding TWT values within the Pliocene, a minimal discrepancy was observed. A similar approach, dictated by similar confidentiality reasons, has already been followed in Tvedt et al. (2013). We have not performed backstripping, due to the uncertainties in the porosity values, derived in turn from geophysical logging; nonetheless, following the results from Maesano et al. (2015), we do not expect systematic changes in the calculated values larger than 15–20%.

Specific software's were used for interpretation, visualization and analysis of the geological features. To facilitate fault analysis, faults were interpreted within the Petrel software environment and exported as mesh surfaces. Subsequently, fault mesh surfaces have been imported in the Move structural geology software for faults displacement analysis. For the along-strike displacement analysis, each horizon's cut-off lines were projected onto the fault plane from a distance of ca. 100 m, in order to avoid underestimation of offset due to dragging in the closeness of the fault plane. Similarly, we calculated along-dip displacement profiles by projecting the horizons on the fault line, on each analysed seismic section.

To sum up the interpretation of the data described above, we here present a conceptual model (Fig. 4) for the interpretation of the faults imaged in the study area. The model faces the propagation of normal faults across an overlying bed that can potentially inhibit the upward propagation of the fault plane. This results in the potential development of a set of cover-restricted faults, accommodating the passive folding on top of underlying fault-propagation normal faults. In this line, we can thus distinguish, with the cover units, between (a) connected faults (i.e., geometrically linked with the underlying main fault): and (b), disconnected or restricted fault (i.e., the lower tip of the overlying fault is clearly separated from the upper tip of the underlying main fault). Down-dip displacement profiles are diagnostic for the recognition of these two types of faults with the cover restriction marked by a significant decrease or null displacement point of the overlying fault, with respect to the typical displacement profile of growing normal faults, with slip increasing downward. These displacement profiles are thus diagnostic also for reconstructing the growth history of the faults and thus to distinguish between connected faults *sensu stricto* and those faults that originated as restricted and later linked downward to the underlying main fault.

Similar to down-dip displacement profiles, along-strike displacement graphs, referenced to specific horizons, can be diagnostic for investigating the along-strike propagation history of each fault strand, including progressive linkage and/or self-similar growth through time. Connected faults show a typical along-strike displacement profiles with older horizons recording more displacement in all the locations along strike. Conversely, restricted segments of faults show a partial inversion of displacement with age, with the clear identification of breach points, suggesting segmentation of the overlying sets of faults.

Subsequently, a comparative analysis was conducted, juxtaposing the findings obtained from the along-dip displacement profile with the shale-to-gouge ratio to investigate the mechanical behaviour of the faults in relation to the lithological composition of the offset units. This

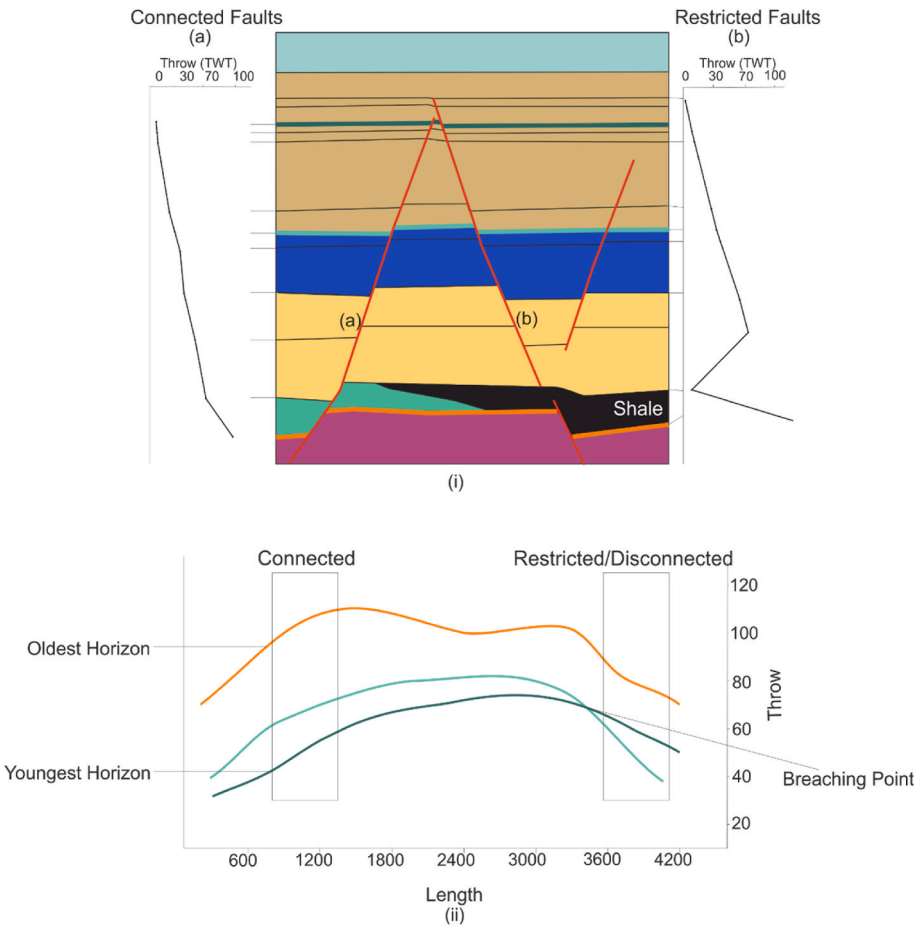

Fig. 4. (i) Conceptual model of fault analysis along dip displacement profiles: a) throw profile of a connected fault; b) throw profile of a fault mechanically restricted/disconnected; (ii) conceptual model of fault analysis along strike displacement profile.

integrative approach allowed us to uncover the underlying factors influencing fault reactivation and further elucidate the complex interplay between fault connectivity and mechanical constraints within the subsurface.

Finally, we inverted the moment tensor solutions of a set of instrumental earthquakes to compare the analysed faults with the present-day stress field. We inverted a total of 25 earthquakes from the RCMT (Regional Centroid Moment Tensor) database (rcmt2.bo.ingv.it; last accessed 06th September 2024; see Supplementary Material). These events have been obtained from the entire time frame of the RCMT catalogue (i.e., from July 01, 1997 to present day) and for the wide region centred on the study area (i.e., 14°-17° east and 41.2° – 42.7° north).

We used both a kinematic method (Linked Bingham kinematic method; FaultKinWin software; Marrett and Allmendinger, 1990) and a dynamic approach (Wintensor software; Delvaux and Sperner, 2003) obtaining the orientation of the principal strain/stress axes and, for the dynamic approach, the stress ratio (i.e., R = [σ2-σ3]/[σ1-σ3]). The obtained stress field has been finally used to calculate the slip tendency of the fault meshes, in the Stress Analysis Module of the MOVE software.

Slip tendency is the ratio of resolved shear stress to resolved normal stress on a surface (Morris et al., 1996). The tendency of a given fault to failure is determined by the ratio of shear stress to normal stress acting on the fault plane and is defined as the slip tendency, ranging from 0 to 1 (e.g., Lisle and Srivastava, 2004; Morris et al., 1996); the greater the calculated slip tendency the more probable failure will be. Given a stress field, slip tendency can be represented on Stereoplots, for any fault plane orientation and on Mohr circles, for a comparison with a Mohr-Coulomb failure curve. For the latter comparison, we assumed an average angle of internal friction of 30° and we showed the failure envelope closer to the calculated Mohr circle, assuming that presently no patches of the faults are slipping, under the present-day stress field. We calculated the absolute values of the principal stresses at the average depth of the Messinian unconformity horizon, and we considered an average density for the Plio-Pleistocene units of 2300 kg/m^3.

4. Results

4.1. Faults network

The structural setting of the study area is influenced by its position near the western tip of the Tremiti strike-slip fault system, contributing to the complex fault network as observed. The faults in the area predominantly display a NW-SE to WNW-ESE orientation, consistently with the regional tectonic trend associated with the Apennines thrust belt and its foredeep. We observed several sets of faults with a normal component of slip on 2D seismic sections. Given that no 3D seismic data are available, no horizontal component can be measured, even if we expect it, considering that the area is located at the western tip of the Tremiti strike slip fault (Fig. 1b). We can group the mapped normal faults into three sets based on the crosscut relationship with the stratigraphic units and their relative orientation with respect to the chain foredeep and forebulge axis (Fig. 5).

*Set*I is composed by high-angle normal faults, striking WNW-ESE (ca. N110), that run longitudinally to chain foredeep and that are displacing only the uppermost levels of the carbonate platform. On top of *Set*I faults, where fault upward propagation is inhibited within the overlying Pliocene shales, a fault-propagation fold develops and secondary high

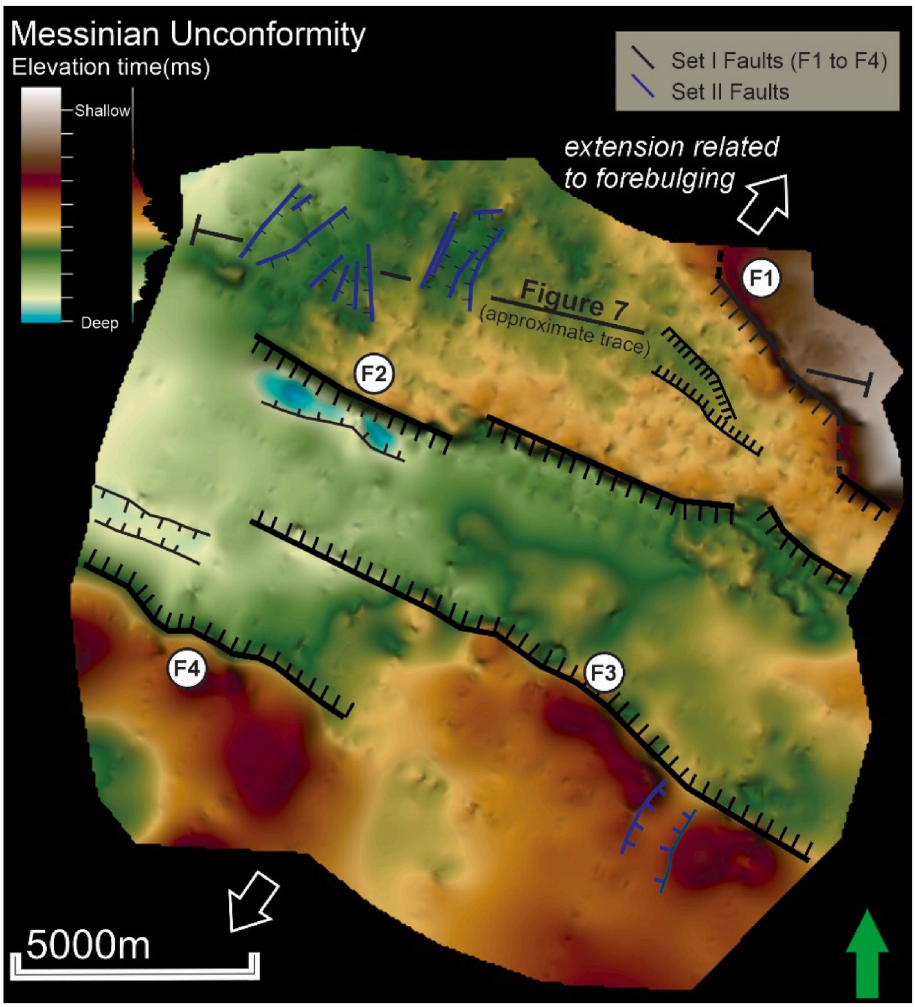

Fig. 5. map of the Messinian horizon along with the 2 sets of faults: the direction of the forebulge-related extension is indicated.

angle normal faults (i.e., bending-moment faults) locally accommodate extension, resulting is cover-restricted faults.

Set II is composed by high angle normal faults, ca. N210 striking, that displace the uppermost part of the carbonate platform. Similar to the major faults, these orthogonal faults are also confined downward by the Messinian Unconformity.

4.1.1. SetI: longitudinal normal faults and overlying cover-restricted faults

*Set*I faults are mechanically restricted faults whose lower tip apparently lies within the carbonate platform. Within the study area, we have identified four major high-angle NW-SE striking normal faults (F1-F4 in Fig. 5) that displace only the uppermost levels of the carbonate platform, with the faulted platform reaching a depth of ca. 1500 msec TWT. In the hanging-wall of F1 and F2, some short synthetic and antithetic faults, mark the bounds of graben-like basins with a maximum length of ca. 4000 m.

As stated above, the lower tip of the structures is restricted within the platform itself (F1 to F4 in Fig. 6), with an average dip of 55–60°, once depth-converted. The small amount of cumulated displacement, the downward dying-out of these faults within the platform and the short-lived evolution: all these features suggest the interpretation of *Set*I faults as due accommodation of extension in the outer arc of the foreland forebulging, migrating across this area through time.

Fault F1 shows some peculiar features, in respect to the other faults populating *Set*I. It has a significantly different strike (N140) and a peculiar zig-zag geometry, where N110 segments show an en-echelon right-stepping pattern, and are connected by N-S striking tracts, each one of ca. 1400 m in length. The minimum length of fault F1, encompassing the study area, is 6.7 km and the maximum fault throw is 152 msec TWT, measured at displaced Messinian unconformity. Due to low resolution with increasing depth, the geometry of F1 beyond ca. 2300 msec TWT within the platform is not clearly visible in the available profiles. However, based on its analogy with other *Set*I faults, F1 seems to be a platform-restricted fault.

Fault F2 is composed of three fault strands, for a total length of 14.6 km, separated by a small left-stepping relay zone, probably hard-linked at depth. Average throw is ca. 90 msec TWT; the maximum value 155 msec TWT is recorded along the western segment. To the west, some antithetic faults are present, ca. 3400 m long, bounding a graben.

Faults F3 and F4 are onshore faults within our study area. F3 spans approximately 13.8 km in length, while fault F4 has a minimum length of approximately 5.5 km. these two faults display a left-stepping en echelon pattern and record and average displacement at the Messinian unconformity of ca. 180 msec TWT.

The faults (F1 and F2) belonging to *Set*I show the tendency to be restricted upwards. In fact, also the upper tip of the faults is typically restricted at the top of the carbonate platform in the footwall block, with faults being apparently inhibited to propagate upward into the Plio-Pleistocene overlying siliciclastic sequence. Instead, these overlying units are involved into typical fault-propagation folds. Nonetheless, as displacement increases, the extension resulting from the overlying folding tends to be accommodated also by localized deformation and a set of cover-restricted normal faults (i.e., bending-moment faults; e.g., Chen et al., 2018) develops in the folded sequence (Fig. 6a and b). The

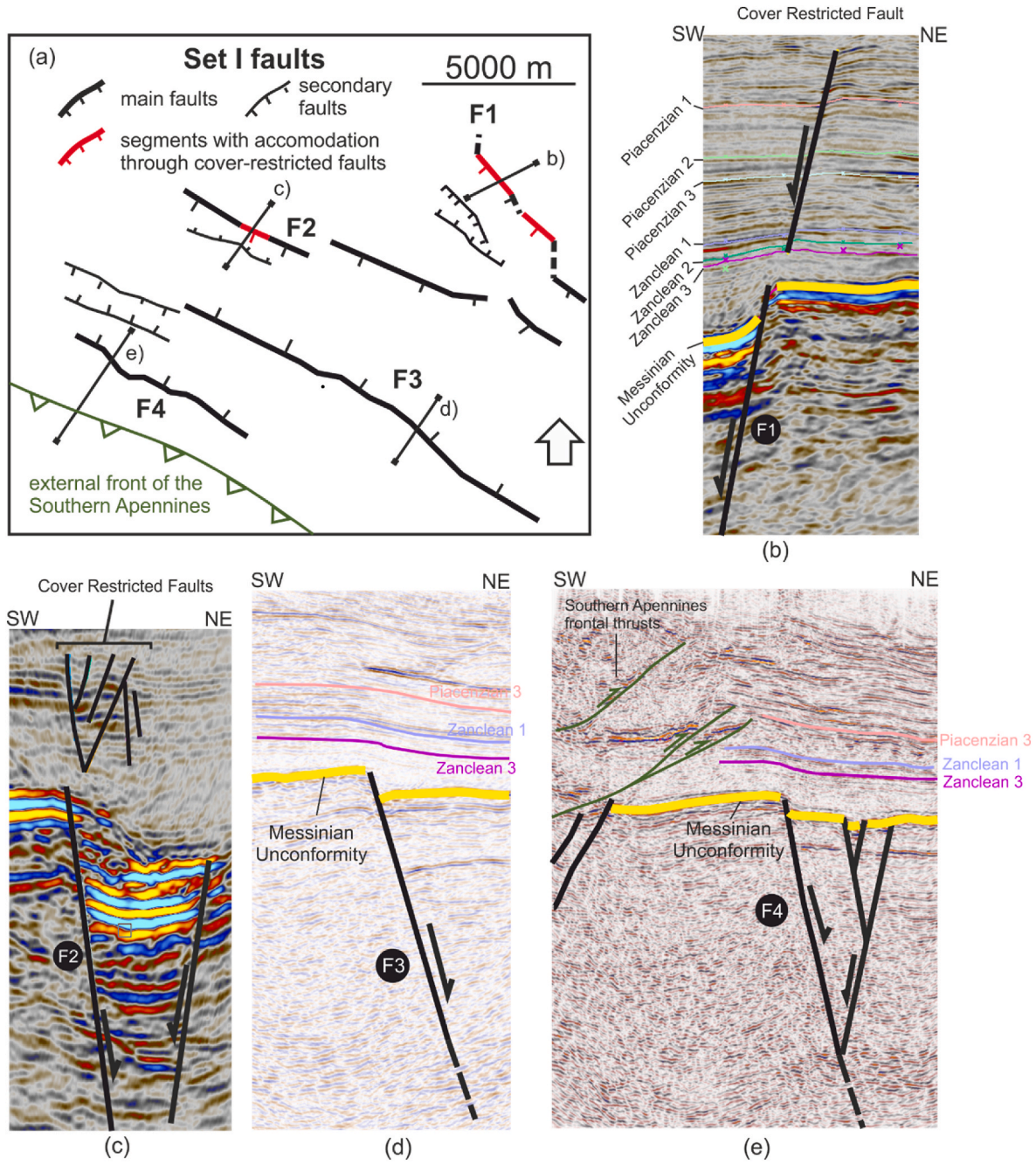

Fig. 6. a) Structural scheme showing the simplified traces of *Set*I faults and the approximate traces of the seismic sections: b) and c) F1 and F2 at locations where a significant offset is cumulated and overlying cover-restricted faults are present; c) F3 fault with a simple and narrow fault zone within the platform and a fault propagation fold above; d) F4, lying in the closeness of the external tip of the Southern Apennines wedge, shows a complex array of synthetic and antithetic faults bound as subsiding basin.

average throw recorded on each of these cover-restricted faults is in the order of a 15–20 msec and can develop small subsiding grabens, close to the anticlinal hinge of the fault-propagation fold.

Our analysis indicates no significant lateral lithological changes near the faults in the Zanclean-Piacentian interval. While differential compaction could be a factor in structural deformation, the available data does not suggest any substantial inhomogeneity in lithology across the study area. Therefore, we interpret the observed downthrow as the result of deep fault reactivation rather than differential compaction effects.

4.1.2. *Set II: orthogonal normal faults*

A second set of faults is composed by numerous short NE-SW striking shallow normal faults, orthogonal to the longitudinal axis of the foredeep and distributed in the north-eastern sector of the study area, in the footwall of F2 and F3 (Fig. 5). These smaller faults are near vertical (dip close to 90°), and the average length is ca. 2 km. The faults are shallow within the carbonate platform and have cumulated throw of only 30 msec TWT, on average.

Faults are arranged into small sets of conjugate faults with near parallel sets bounding structural grabens elongated in the same direction. At depth these faults are still almost vertical and can be recognised until ca. 400 msec TWT (Fig. 7), probably due to the loss in vertical

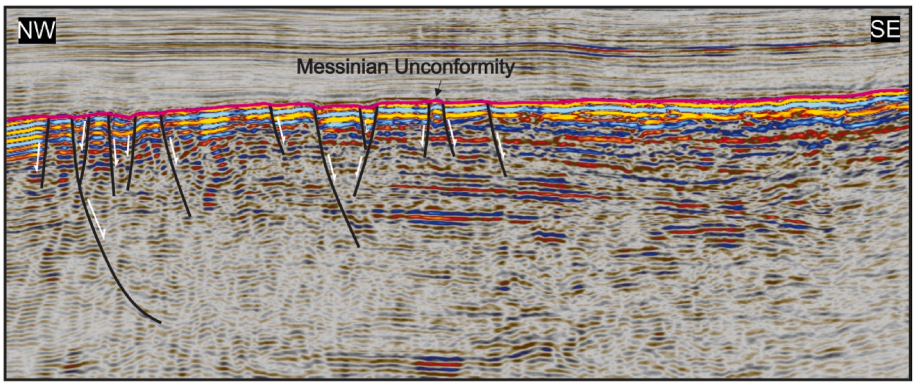

Fig. 7. Set II of orthogonal shallow normal faults located in the hanging wall of fault F2.

resolution of the seismics at those intervals.

4.2. *Structural maps and fault displacement analysis: the Neogene evolution of the fault sets*

Thickness maps of the intervals between the interpreted horizons (Messinian, Zanclean 2, Zanclean 1, Piacenzian 3, Piacenzian 2, Piacenzian 1) within the foredeep sequence (Fig. 3) provides a plan view picture of the evolution of the fault network since Early Pliocene times (Fig. 8).

*Set*I faults include the main tectonic structures deforming the area during the Zanclean (Fig. 8b and c), with F2 and F3 showing evidence of fault activation only in the Western section of the map. During this interval, antithetic *Set*I faults developed in narrow sectors near the traces of F2 and F3, where significant variations in displacement along the fault length indicate localized tectonic stress.

Between Zanclean 1 and Piacenzian 3 (i.e., early Piacenzian), the faults were almost inactive, with some possible movements along fault F2 (Fig. 8d).

Later, during the Piacenzian (Fig. 8e), faults have been re-activated, particularly in the western sector of the study area (F3 and F4), with the subsequent development of a narrow fast-subsiding basin. Finally,

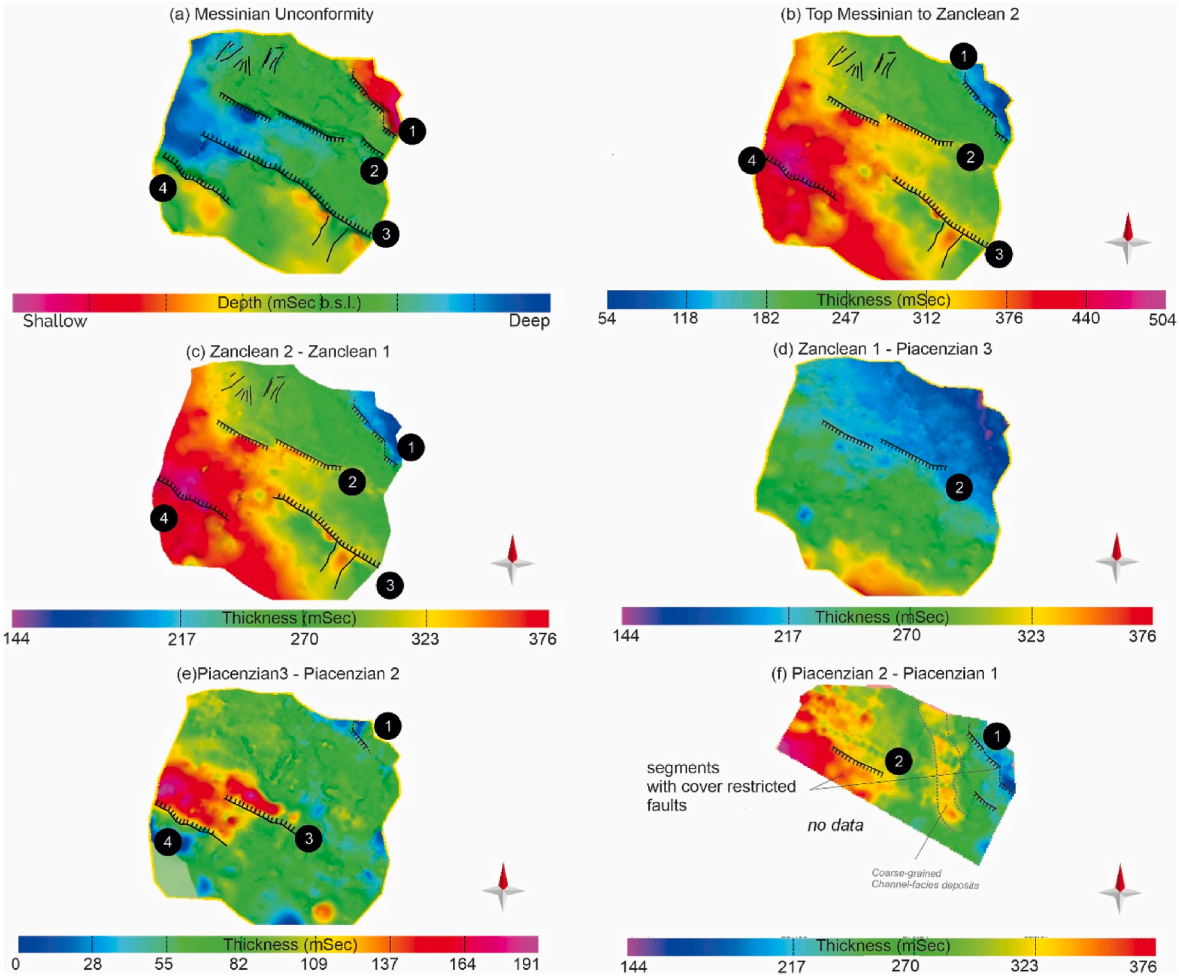

Fig. 8. (a) Isobaths (depth contours) and (b–f) isopaches (thickness contours) both in TWT for horizons and the intervals between horizons in the study area.

during the latest Piacenzian (Fig. 8f), the deformation moved in the eastern side of the study area, especially along F1, whereas F2 showed only a minor re-activation. No data are available for the onshore sectors (F3 and F4). During this period, the local re-arrangement of submarine channels, resulted in the deposition of a thick coarse-grained channel-facies body, running almost N-S across the study area (Fig. 8f).

Fault F2 shows evidence of reactivation in a single seismic line (Fig. 6b). This line shows the presence of a narrow graben with a complex set of cover-restricted faults accommodating the extension above the tip of the main synthetic structure. Given the limited dataset covering this evidence, the fault will not be analysed thoroughly here.

Conversely, fault F1 is the best documented structure in our dataset, showing a complete record in several seismic reflection lines and, will be analysed in detail. Along the fault F1, the strike shows a recent reactivation, resulting in folding of the overlying units and in the development of cover restricted faults, above the tip of the main structure.

The along-dip displacement profile of F1 (Fig. 9) reveals an abrupt decrease in throw at the top of Messinian unconformity, followed by an uneven displacement pattern in the overlying cover units. Two displacement peaks are observed at the Piacenzian 2 and Zanclean 2 horizons reaching a max throw of 17 msec TWT and 14 msec TWT, respectively. In contrast, the horizons Piacenzian 3 and Zanclean 3 show smaller displacements, measuring approximately 6 msec and 8 msec TWT. As conceptually illustrated in the Methods Section, this displacement profile indicates a cover-restricted fault strand that accommodated slip induced by movement on the underlying fault F1. Localized displacement is particularly inhibited within the Zanclean and close to Piacenzian 3 horizon.

The comparison with lithological facies, as derived from gamma ray-logs (Fig. 9) clearly correlates the abrupt decrease in localized displacement to the presence of shale layers. These end to accommodate offset through folding and/or distributed sub-seismic small-scale faults, rather than allowing an upward propagation of fault tip.

The along-strike displacement profile (Fig. 10) illustrates important changes of such a behaviour along the strike of the fault. The Messinian has cumulated the highest amount of displacement, with a bimodal profile of along-strike throw that clearly defines two presently linked segments within the fault, with a maximum displacement of 152 msec TWT. Despite the hard-linkage of the two segments, important changes in the cumulative throw distribution are still visible along strike also in the youngest horizons, particularly in the area between 1500 and 2000 m (Fig. 10), suggesting that structural segmentation persisted also after linkage. The along-strike throw distribution with time, in fact, shows that a progressive filling of the throw gap with time was inhibited, promoting instead a persistent segmentation of the fault through a barrier located between the two old segments.

Following these observations, we identified two distinct segments, denoted as Segment A, to the northwest, and Segment B, to the southeast (Fig. 10a). Notably, Segment A exhibits a well-connected fault system, whereas Segment B is characterized by the presence of cover-restricted faults, above fault F1. Segment B can be further subdivided into two subsectors: one featuring a single-layer restriction and the other manifesting a multi-layer restriction. Within the single-layered restriction subsector, it is observed that the inversion of the Piacenzian 2 and 3 exceeds that of the Zanclean 1 and 2, with a segment where Piacenzian inversion is notably absent. In this multi-layered restriction zone, inversions are observed in both the Zanclean and Piacenzian horizons. Segment A exhibits the maximum fault throw during the Zanclean, whereas Segment B shows the maximum throw during the Piacenzian.

This is better illustrated in Fig. 10b, where we mapped the distribution of throw along the fault plane, projected as vertical. The segmentation of the fault F1 is clearly depicted both at depth and in the shallower portion of the fault, where the limited amount of displacement migrated toward the southeast (toward Segment B), through time.

4.3. Earthquake data inversion and slip tendency of the fault network

The inversion of the available earthquake focal mechanisms in the area can be used to investigate if changes in the local stress field is one of the main factors controlling the selection of more compliant fault segments to be re-activated during the latest tectonic phase, under the assumption that the stress field has remained stable since Late Pliocene. We selected events located within a significant area around the study area, including the margin of the Middle Adriatic Ridge (MAR), the Tremiti Fault Zone and Mattinata Faults.

Fig. 11a displays the available focal mechanisms, mainly represented by strike-slip or thrust faulting events. The inversion of the data reveals a strike-slip regime with a maximum horizontal stress axis bearing NW-SE (Table 1).

The slip tendency has been calculated on the three-dimensional mesh surfaces obtained from interpreted seismic data for main faults in the area (Fig. 11b). Slip tendency shows significant changes along the length of the faults, mainly due to small changes in the faults strike.

Fault F1 is the most prone to slip along its entire length and downdip extent. F2, F3 and F4 show more complicated patterns, with more compliant segments alternating with other ones less prone to slip, under

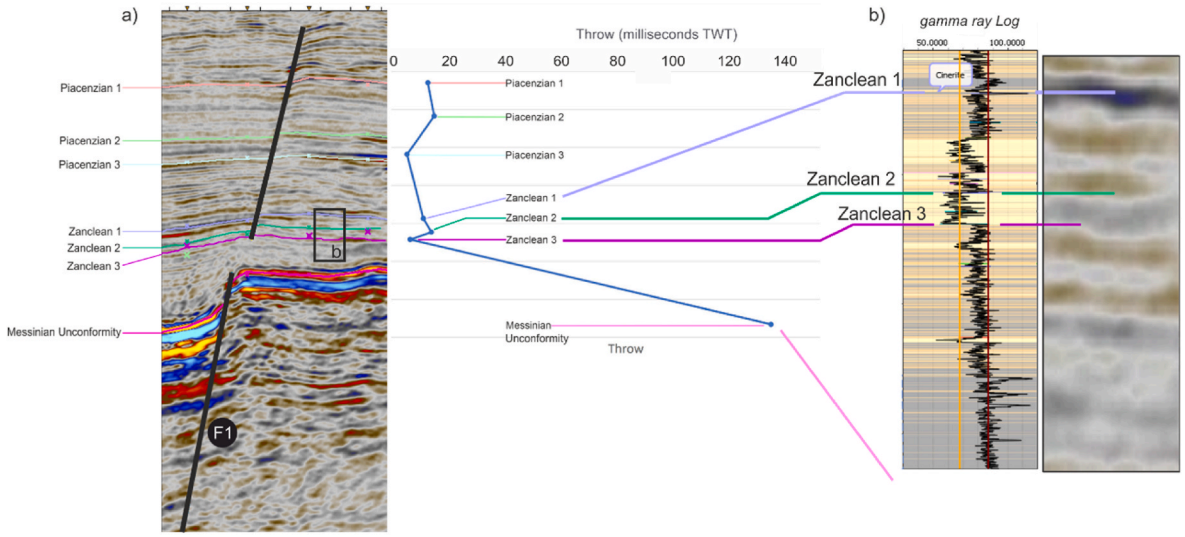

Fig. 9. Along-dip displacement profile of the fault F1: note the abrupt decrease of displacement along the profile, pointing to the presence of a cover restricted fault.

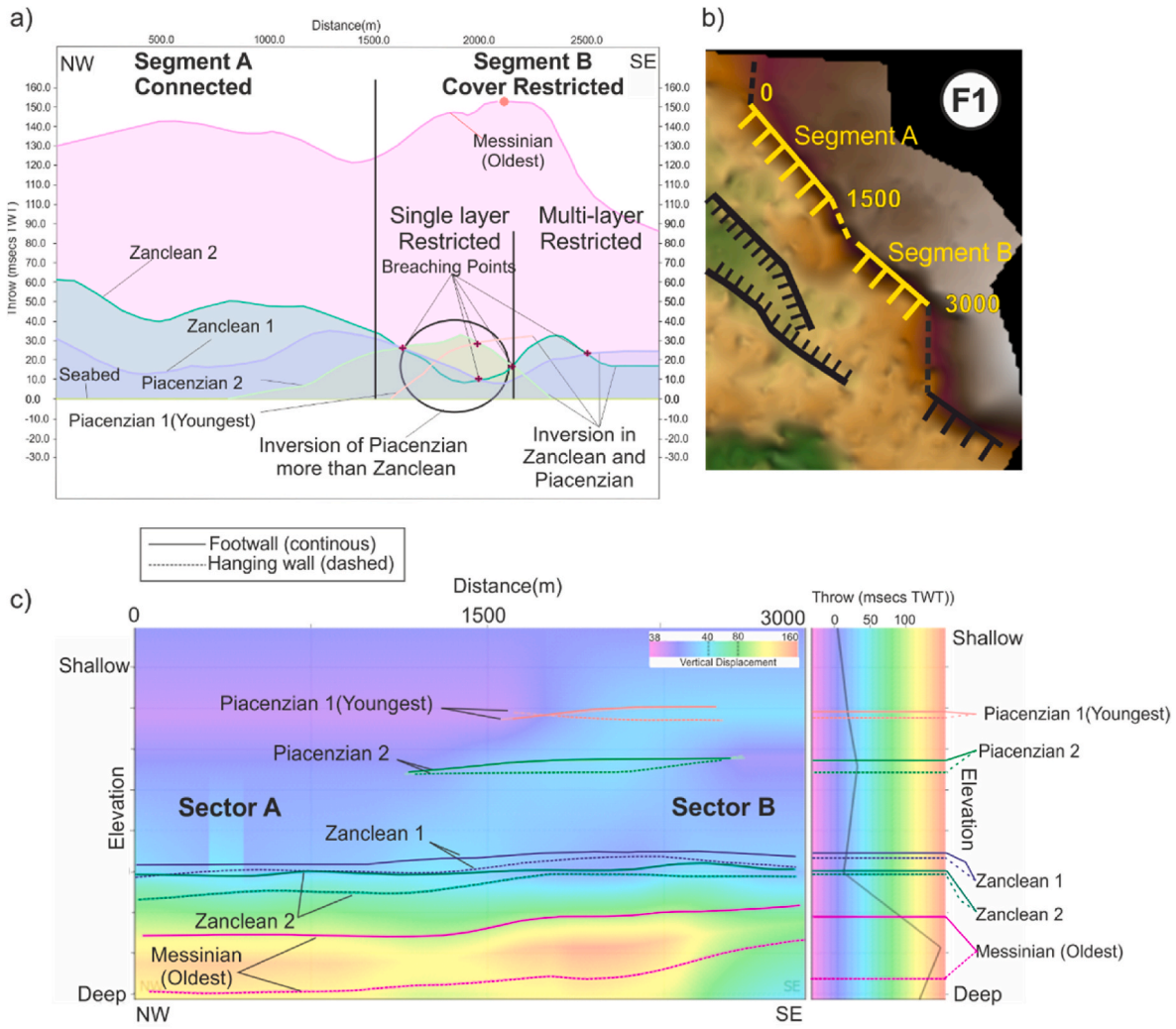

Fig. 10. a) along strike displacement analysis of Fault F1, along the sector marked in yellow on map in b); c) interpolated throw distribution along the fault plane: cutoffs of the mapped horizons are highlighted (dashed lines for hanging wall and continuous lines for the footwall). (For interpretation of the references to colour in this figure legend, the reader is referred to the Web version of this article.)

the present-day stress field. In particular, F2 shows a high slip tendency in its southernmost part. The fault segments more prone to slip are those ones displaying high dip angles and striking N100–110 or N140-150 (Fig. 11b).

Notably, those segments more predisposed to slip are the ones that moved during the latest tectonic phase, thus confirming the initial assumption, that the area experienced a stable tectonic stress field since Late Pliocene to present day.

5. Discussion

Drawing on the data described above, we finally discuss how structural inheritance influences the development of later faulting network and then analyse the strain localization and faulting style within a mechanically layered sequence.

5.1. Faults re-activation from forebulging to transtensional tectonics

During a first tectonic phase (Fig. 12a), the area underwent a ca. N40 directed extension, accommodating the forebulging at the front of the Southern Apennines (Fig. 5). The time encompassed by this first tectonic phase in the study area can be constrained between Messinian and the late Zanclean, based on thickness maps, and ended in the late Zanclean, with a period of relative tectonic quiescence until the Piacenzian.

At the same time, also faults F2, F3 and F4 developed as optimally oriented *Set*I faults, restricted within the Apulian platform. Set II faults, given their limited length and cumulate displacement, can likely be interpreted as footwall release faults (*sensu* Destro, 1995) that accommodate footwall strain where a high displacement gradient is present of the main fault. We observe, especially for those faults located in the footwall of F2 (Fig. 5), that on the main longitudinal fault a small sector with a high cumulative displacement and a short graben structure is present in their closeness. Additionally, Set II faults dip in the direction where displacement decrease along the main fault, consistently with kinematics of release faults.

Assuming the foredeep-forebulge system migration velocity of 15 mm/yr (Sabbatino et al., 2021), this could had moved 15–20 km in the time interval between the latest activity of Zanclean tectonic phase and the inception of the first pulses of the second one. Such a distance had possibly resulted in the bypass of the study area by the forebulge and in the generalized rest of the previously active normal faults.

During the successive tectonic phase (Piacenzian to present-day; Fig. 12b) we record the re-activation of selected segments of the fault network under a new tectonic stress field. We interpret this drastic change as due to the incorporation of this area in the eastern tip of the Tremiti Fault Zone with a horse-tail and extensional normal faults (Kim and Sanderson, 2006). Notably, the timing of inception of this tectonic phase is consistent with the age of the latest tectonic phase recorded at

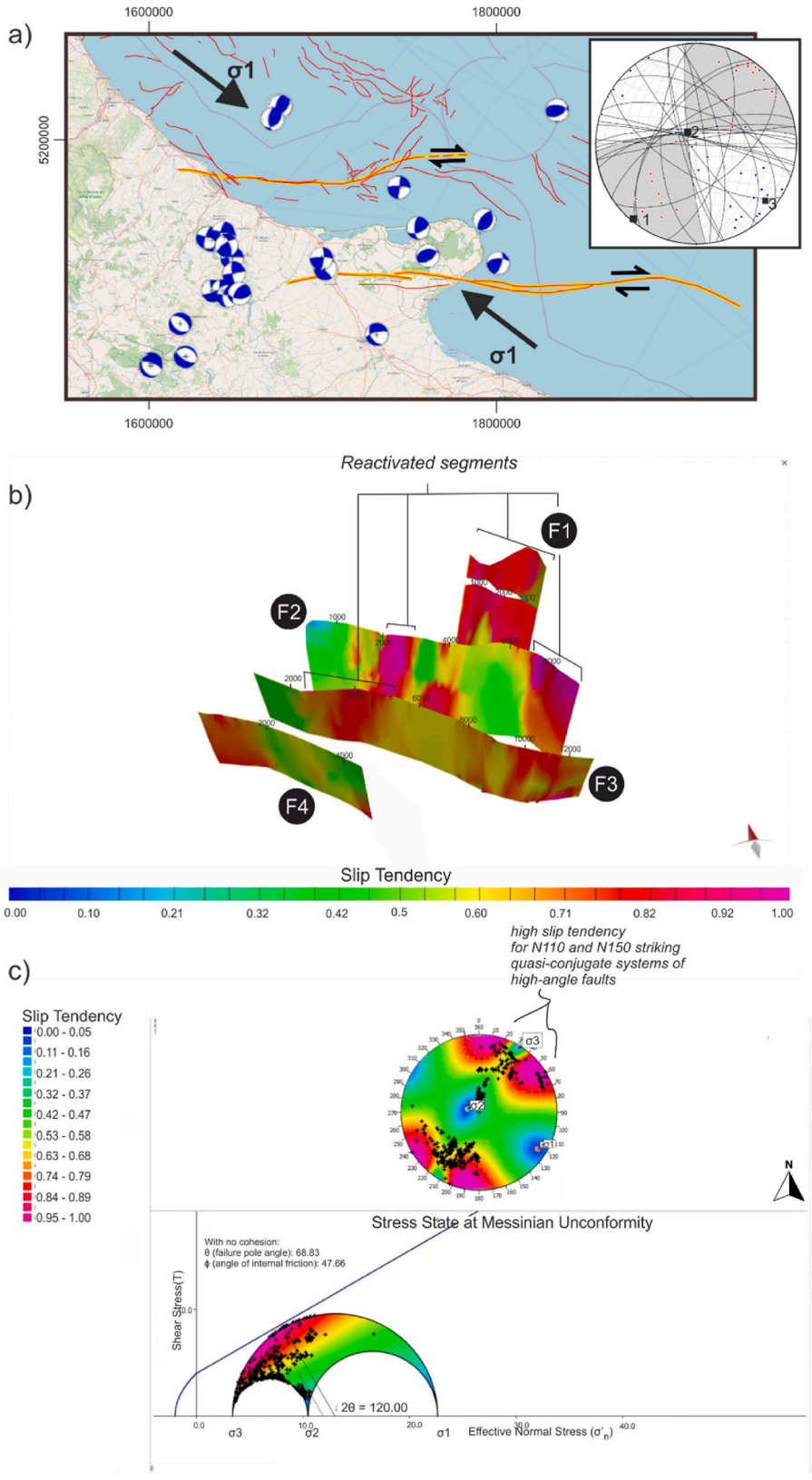

Fig. 11. a) Earthquake focal mechanisms and results from the kinematic inversion (P and T axes and kinematic axes are plotted together with the resulting best fit fault plane solution); b) calculated slip tendency plotted onto the faults' surfaces and c) stress state, calculated at the depth of the Messinian unconformity, represented in the stereo-diagram and Mohr circle graphs.

Table 1
strain axes calculated following the kinematic (Marrett and Allmendinger, 1990) and the dynamic method (Delvaux and Sperner, 2003).

Strain Axis	Trend/plunge	Stress axis	Trend/plunge
		Stress ratio (R) = 0.37	
E1	*220/03*	*σ3*	*220/01*
E2	*323/79*	*σ2*	*314/76*
E3	*130/11*	*σ1*	*129/14*

the Tremiti islands (Brozzetti et al., 2006, Fig. 1b).

The normal component of displacement observed at this stage and the geometry of the fault array, would be reconciled with the calculated strike slip tectonic environment, if we consider the area as representing the easternmost termination of the dextral strike slip Tremiti Fault Zone. The described fault geometry and architecture is consistent with the termination of large deep-seated wrench zones, where distributed strain is locally accommodated by horsetail sets of faults (Sylvester, 1988; Morley, 2002; Kim and Sanderson, 2006). It is commonly observed that these faults can strike at high angle with respect to the main shear zone and that are typically located in the dilational quadrant of the fault tip (Segall and Pollard, 1980).

Fault plane orientation is apparently the main factor determining the extent of fault re-activation, during this stage, if we compare the tracts with evidence of later re-activation with the predicted present-day stress field. In this line, inherited fault from the Zanclean tectonic phase, accommodated deformation only in those sectors where are compliant. Fault F1, that previously developed with a non-optimal orientation,

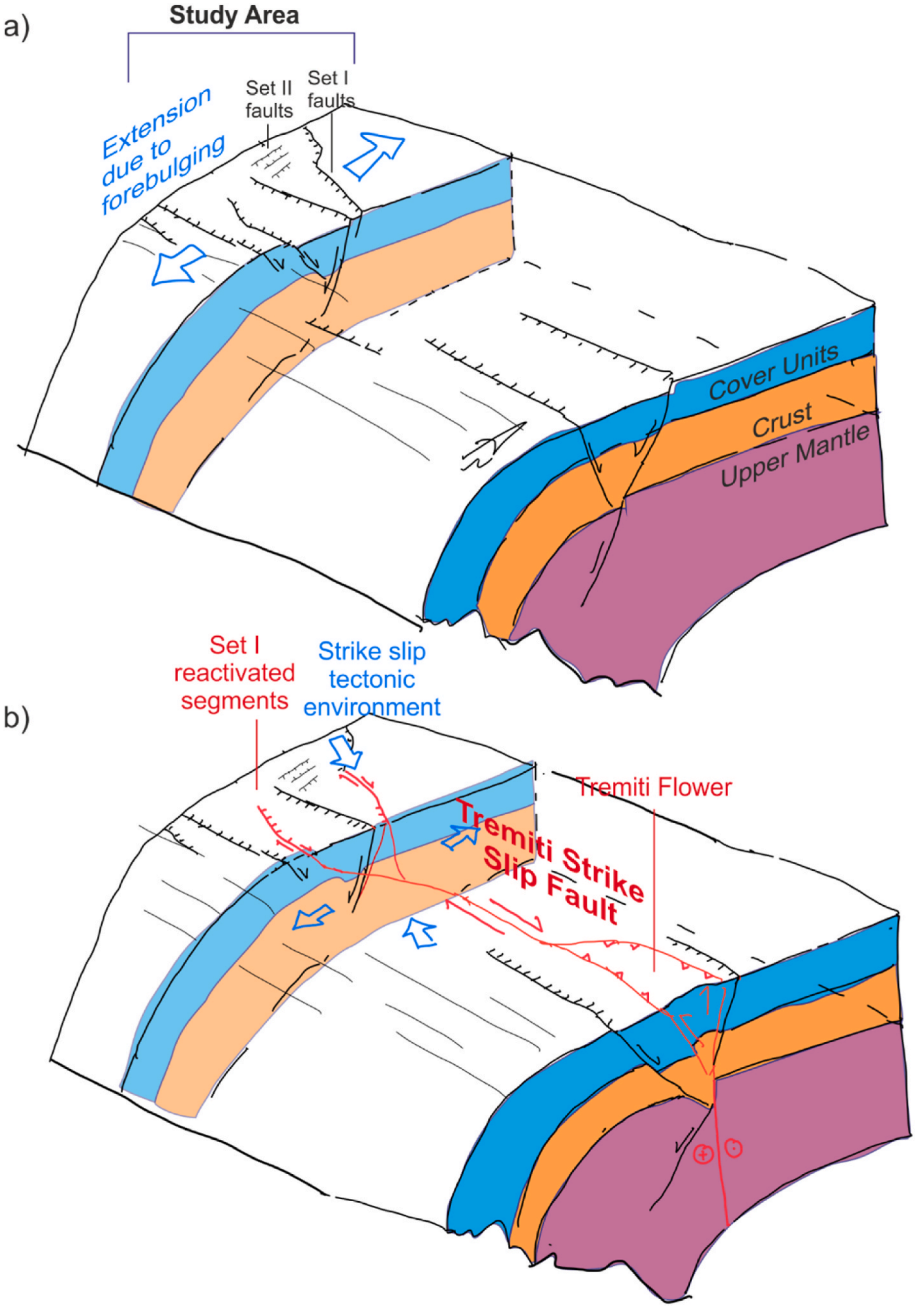

Fig. 12. Conceptual scheme summarizing the tectonic evolution of the study area and surroundings sectors: a) Zanclean tectonic phase, dominated by normal faults accommodating outer arc extension due to forebulging; b) Piacenzian tectonic phase, characterized by the re-activation of compliant inherited fault segments, under a strike slip tectonic environment.

driven by inherited crustal weakness zones, was later better oriented for re-activation, resulting in the later linkage of the two fault strands developed so far and in the localization of most of the deformation recorded in the area.

The other faults, conversely, experienced a very limited re-activation, focused in the relay zones of F2, where a more compliant geometry is present. Lacking three-dimensional kinematics on the set of the analysed faults, we can only rely on dip slip kinematics, that can be potentially largely underestimating the real amount of fault displacement, for progressively more oblique rake values.

Complex fault patterns have been described and modelled for wrench zones (Naylor et al., 1986; Sylvester, 1988), including the characterization of the complex wrench zone belonging to the Mattinata Fault, some kilometres to the south, where the strike slip fault is interacting with the advancing front of the Southern Apennines (Di Bucci and Mazzoli, 2003; Tondi et al., 2005; Di Bucci et al., 2006). In areas located at the fault tips, both transpressive and transtensive tectonics are predicted, mainly depending on i) their location within the dilational or compressional quadrants, ii) the possible interactions with other concurrent deforming fronts (Di Bucci et al., 2006) and iii) possible interactions with inherited faults, with high-angle structures mostly associated with transtensional accommodation (Sylvester, 1988; Kim and Sanderson, 2006).

It is noteworthy that, however, the faults re-activated under strike slip tectonics, are apparently still restrained within the Apulian Platform, thus accommodating only the shallow deformation into the crustal volume. This would imply the existence of a weak detachment level, where decoupling between the upper platform units and the lower ones can be obtained. We propose that the Burano anhydrites, at the base of the Apulian Platform, are a well-fitting candidate as such a weak layer. Several diapiric structures, localized in the foreland or along the Middle Adriatic Ridge are known and fed by the Burano anhydrites. The thickness and lithology of the Burano anhydrites below the Apulian Platform is unknown: this units has been directly explored at very limited outcrops (e.g., Bosellini et al., 1999) and, in the subsurface, through limited well-cores (e.g., Scisciani and Esestime, 2017; Borrelli et al., 2023), including the some deep exploration wells, some kilometers from the study area (i.e., “Androdoco 1” “Gargano 1”, “Ernesto Nord 1” “Puglia 1” and “Foresta Umbra 1” wells; available at the Videpi database webpage – https://www.videpi.com/videpi/pozzi/pozzi.asp; last accessed on the 12th Jan 2024).

Additionally, the Mattinata and Tremiti Faults are both apparently young structures that accommodated a relatively small amount of displacement (Tondi et al., 2005; Brozzetti et al., 2006; Di Bucci et al., 2006), conversely to what has been originally speculated by previous Authors (De Dominicis and Mazzoldi, 1987). Structurally immature faults tend to accommodate only a small portion of the slip at depth near the surface (ca. 50–60%, according to Dolan and Haravitch, 2014) and typically display a distributed strain accommodation at relatively shallow depths.

5.2. *Influence of mechanical layering on cover-restricted faults’ initiation and growth*

Albeit several segments of the fault network experienced a later re-activation, only very limited sectors display the presence of cover-restricted faults. Most of the offset from underlying main faults is accommodated in the overlying foredeep units through folding and/or sub-seismic localized deformation.

Cover-restricted faults develop only where offset on the main fault is large and/or the presence of grabens locally enhance the throw on the main synthetic normal fault thus resulting in the development close growth folds, over propagating normal faults (Coleman et al., 2019). When folding exceeds a threshold value, given by the fold wavelength and thickness of the folded units (Livio et al., 2018), bending-moment faults enucleate near the anticlinal hinge of the folds. These enucleates as isolated small shear fractures within the layers that are mechanically predisposed to localize deformation (i.e., more sandy layers) and then tend to propagate as double-edge restricted faults (Soliva and Benedicto, 2005; Soliva et al., 2006; Tavani et al., 2006; Roche et al., 2012), as elsewhere already observed in similar setting (Bull et al., 2006; Bitonte et al., 2021).

When analyzing along-dip displacement profiles, we observed that maximum displacement of cover restricted faults is multimodal, with two maxima located within the Zanclean and in the middle of the Piacenzian interval. We can suppose that maxima along profiles indicate the enucleation point of the initial fault, even if considering that other factors (e.g., fault interactions) can concur in determining the cumulative displacement profile through time (Bürgmann et al., 1994; Cowie and Shipton, 1998; Wilkins and Gross, 2002). Notably, lithologies characterized by: i) high porosity, ii) low cementation, iii) high ductility, iv) a relatively high clay/organic/evaporite mineral content and v) a strain-softening dynamic behavior tend to experience a higher pre-faulting strain before fault nucleation and to inhibit a later fault propagation with slip (e.g., Van Gent et al., 2010; Agosta et al., 2015; Ferrill et al., 2017). In our setting, shales behave as a decoupling level, promoting folding and distributed accommodation and resulting in a higher displacement gradient (e.g., McGinnis et al., 2016; Ferrill et al., 2012). The lower Zanclean interval, for example, show a strongly asymmetric profile, with a marked lower fault tip gradient, suggesting that upward fault tip propagation strongly inhibited at the upper tip.

6. Conclusions

We analysed a sector of the foredeep system of the Southern Apennines that can be considered as paradigmatic of a foreland sector involved into different successive tectonic phases during the Neogene.

By means of thickness and displacement analysis, we explored the evolution of the fault network through time and in space: we investigated the factors controlling fault re-activations and propagation in the thick cover units and compared the present-day tectonic stress field with the latest faults re-activations.

From the data and analysis above, the following conclusions can be drawn.

- a change in the tectonic stress field from forebulge-related extension to a strike slip tectonic environment can be dated back after Pliocene, when the area was incorporated at the tip of the right-lateral Tremiti Fault Zone;
- in this area, characterized by a limited deformation and where faults experienced relatively small amount of displacement through time, fault plane orientation is the main factor determining the potential for fault re-activation as strike-slip or normal faults.
- the propagation of normal faults into the overlying foredeep sequence is mostly inhibited by such a thick sequence of clastic units. Nonetheless, at places, fault propagation can be promoted by large offset on the main faults and/or my closer growth folds, with the development of cover-restricted bending-moment faults.

Foredeep settings are of primary importance for oil & gas plays exploitation and for gas storage projects, often to be developed in depleted reservoir. Nonetheless, a deep and careful structural and mechanical characterization is needed, as underlined in the present study. We demonstrate that significant changes in structural style, fault connectivity and partitioning of deformation happen at small distances along the structural network, depending on both stress state and on mechanical stratigraphy of the overlying cover units.

Funding

This research was supported by funding from the **European Union – NextGenerationEU – Mission 4 “Education and Research” –**

Component 2 "From Research to Business" – Investment 3.1 "Fund for the realization of an integrated system of research and innovation infrastructures" – Project IR0000037 – GeoSciences IR.

CRediT authorship contribution statement

Frank Thomas: Writing – original draft, Visualization, Validation, Software, Methodology, Investigation, Formal analysis, Data curation, Conceptualization. **Franz A. Livio:** Writing – review & editing, Validation, Supervision, Resources, Project administration, Methodology, Formal analysis, Conceptualization. **Norberto De Marchi:** Supervision, Resources, Project administration, Funding acquisition. **Raffaele Bitonte:** Writing – review & editing, Supervision, Software, Resources, Project administration, Investigation.

Declaration of competing interest

The authors declare that they have no known competing financial interests or personal relationships that could have appeared to influence the work reported in this paper.

Acknowledgements

This manuscript has been greatly improved thanks to the reviews and the suggestions by Prof. Vittorio Scisciani and Dr. Gang Rao.

We would like to express our sincere gratitude to Energean for their invaluable support and collaboration during this study. Their provision of datasets, reports, and detailed stratigraphic characterization significantly expedited our research progress. Seismic interpretation has been performed by means of the Petrel software, under Academic license, courtesy of SLB (Schlumberger); structural analysis and slip tendency analysis have been performed by means of the MOVE suite software, under Academic license, courtesy of Petex (Petroleum Experts).

Data availability

The data that has been used is confidential.

References

Agosta, F., Wilson, C., Aydin, A., 2015. The role of mechanical stratigraphy on normal fault growth across a Cretaceous carbonate multi-layer, central Texas (USA). Italian Journal of Geosciences 134 (3), 423–441.

Agosta, F., Petrullo, A.V., La Bruna, V., Prosser, G., 2023. Cenozoic Fault growth mechanisms in the outer apulian platform. Geosciences 13, 121.

Ahmadhadi, F., Lacombe, O., Daniel, J.-M., 2007. Early reactivation of basement faults in central zagros (SW Iran): evidence from pre-folding fracture populations in asmari formation and lower tertiary paleogeography. In: Lacombe, O., Roure, F., Lavé, J., Vergés, J. (Eds.), Thrust Belts and Foreland Basins, Frontiers in Earth Sciences. Springer, Berlin, Heidelberg, pp. 205–228. https://doi.org/10.1007/978-3-540-69426-7_11.

Anderson, H., 1987. Is the adriatic an african promontory? Geology 15, 212–215.

Anzidei, M., Baldi, P., Casula, G., Pondrelli, S., Riguzzi, F., Zanutta, A., 1997. Geodetic and seismological investigation in the Ionian area. Ann. Geophys. 40 (5).

Argnani, A., Frugoni, F., 1997. Foreland Deformation in the Central Adriatic and its Bearing on the Evolution of the Northern Apennines.

Argnani, A., Gamberi, F., 1995. Stili strutturali al fronte della catena appenninica nell'Adriatico centro-settentrionale. Studi Geol. Camerti 1995, 19–27.

Bally, A.W., 1986. Balanced sections and seismic reflection profiles across the Central Apennines. Mem. Soc. Geol. It. 35, 257–310.

Barchi, M.R., Tavarnelli, E., 2022. Thin vs. Thick-Skinned Tectonics in the Umbria-Marche Fold-And-Thrust Belt: Contrast or Coexistence?.

Battaglia, M., Murray, M.H., Serpelloni, E., Bürgmann, R., 2004. The Adriatic region: an independent microplate within the Africa-Eurasia collision zone. Geophys. Res. Lett. 31.

Billi, A., Salvini, F., 2003. Development of systematic joints in response to flexure-related fibre stress in flexed foreland plates: the Apulian forebulge case history, Italy. J. Geodyn. 36, 523–536. https://doi.org/10.1016/S0264-3707(03)00086-3.

Bitonte, R., Livio, F.A., Mazzoli, S., Bellentani, G., Di Cesare, L., Dall'Igna, M., et al., 2021. Frontal accretion vs. foreland plate deformation: discriminating the style of post-collisional shortening in the Apennines. J. Struct. Geol. 145, 104290.

Borrelli, M., Perri, E., Morsilli, M., Critelli, S., 2023. Late Permian-Triassic sedimentary evolution of the Southern Adriatic area based on wells and cores analysis. Mar. Petrol. Geol. 150, 106154.

Boschi, E., Guidoboni, E., Ferrari, G., Mariotti, D., Valensise, G., Gasperini, P., 2000. Catalogue of strong Italian Earthquakes from 461 BC to 1997 (Appendix). Ann. Geophys. 43 (4).

Bosellini, A., Morsilli, M., Neri, C., 1999. Long-term event stratigraphy of the Apulia platform margin (upper jurassic to Eocene, Gargano, southern Italy). J. Sediment. Res. 69 (6), 1241–1252.

Brozzetti, F., D'Amato, D., Pace, B., 2006. Complessità delle deformazioni neogeniche nell'avampaese adriatico: nuovi dati strutturali dalle Isole Tremiti. Rendicont. Soc. Geol. Ital. 2, 94–97.

Bull, J.M., Barnes, P.M., Lamarche, G., Sanderson, D.J., Cowie, P.A., Taylor, S.K., Dix, J. K., 2006. High-resolution record of displacement accumulation on an active normal fault: implications for models of slip accumulation during repeated earthquakes. J. Struct. Geol. 28, 1146–1166. https://doi.org/10.1016/j.jsg.2006.03.006.

Bürgmann, R., Pollard, D.D., Martel, S.J., 1994. Slip distributions on faults: effects of stress gradients, inelastic deformation, heterogeneous host-rock stiffness, and fault interaction. J. Struct. Geol. 16, 1675–1690.

Butler, Robert W.H., Mazzoli, S., 2006. Styles of continental contraction: a review and introduction. In: Mazzoli, S., Butler, R.W.H. (Eds.), Styles of Continental Contraction. Geological Society of America. https://doi.org/10.1130/2006.2414(01, 0.

Butler, R.W.H., Tavarnelli, E., Grasso, M., 2006. Structural inheritance in mountain belts: an Alpine–Apennine perspective. Journal of Structural Geology, Tectonic Inversion and Structural Inheritance in Mountain Belts 28, 1893–1908. https://doi.org/10.1016/j.jsg.2006.09.006.

Calamita, F., Cello, G., Centamore, E., Deiana, G., Micarelli, A., Paltrinieri, W., Ridolfi, M., 1991. Stile deformativo e cronologia della deformazione lungo tre sezioni bilanciate dell'Appennino umbro-marchigiano alla costa adriatica. STUDI GEOLOGICI CAMERTI. NUOVA SERIE, pp. 295–314.

Carboni, F., Mirabella, F., Minelli, G., Saleh, H., Porreca, M., Ercoli, M., Pauselli, C., Barchi, M.R., 2024. Kinematic reconstruction of active tectonic and halokinetic structures in the 2021 NW Palagruža earthquake area (Central Adriatic). J. Struct. Geol. 182, 105112. https://doi.org/10.1016/j.jsg.2024.105112.

Casero, P., Bigi, S., 2013. Structural setting of the Adriatic basin and the main related petroleum exploration plays. Mar. Petrol. Geol. 42, 135–147. https://doi.org/10.1016/j.marpetgeo.2012.07.006.

Casero, P., Roure, F., 1994. Neogene deformations at the Sicilian–North African plate boundary. Peri-Tethyan Platforms, pp. 27–50.

Cavinato, G.P., Cosentino, D., Funiciello, R., Parotto, M., Salvini, F., Tozzi, M., 1994. Constraints and new problems for geodynamical modelling of central Italy (CROP 11 Civitavecchia-Vasto deep seismic line). Boll. Geofis. Teor. Appl. 36, 159–174.

Chen, Li, T., Thompson Jobe, J., Burbank, J.A., Cheng, D.W., Xu, X., Li, J.Z., Zheng, W., Zhang, P., 2018. Active bending-moment faulting: geomorphic expression, controlling conditions, accommodation of fold deformation. Tectonics 37, 2278–2306. https://doi.org/10.1029/2018TC004982Coleman.

Coleman, A.J., Duffy, O.B., Jackson, C.A.L., 2019. Growth folds above propagating normal faults. Earth-Sci. Rev. 196, 102885.

Cosentino, D., Cipollari, P., Marsili, P., Scrocca, D., 2010. Geology of the central Apennines: a regional review. J. Virtual Explor. 36. https://doi.org/10.3809/jvirtex.2010.00223.

Coward, M.P., De Donatis, M., Mazzoli, S., Paltrinieri, W., Wezel, F.-C., 1999. Frontal part of the northern Apennines fold and thrust belt in the Romagna-Marche area (Italy): shallow and deep structural styles. Tectonics 18, 559–574.

Cowie, P.A., Shipton, Z.K., 1998. Fault tip displacement gradients and process zone dimensions. J. Struct. Geol. 20, 983–997. https://doi.org/10.1016/S0191-8141(98)00029-7.

Craddock, J.P., Malone, D.H., Porter, R., Compton, J., Luczaj, J., Konstantinou, A., Day, J.E., Johnston, S.T., 2017. Paleozoic reactivation structures in the Appalachian-Ouachita-Marathon foreland: far-field deformation across Pangea. Earth Sci. Rev. 169, 1–34. https://doi.org/10.1016/j.earscirev.2017.04.002.

Critelli, S., Muto, F., Tripodi, V., Perri, F., Schattner, U., 2011. Relationships between lithospheric flexure, thrust tectonics and stratigraphic sequences in foreland setting: the Southern Apennines foreland basin system, Italy. Tectonics 2, 121–170.

De Dominicis, A., Mazzoldi, G., 1987. Interpretazione geologico-strutturale del margine orientale della piattaforma apula. Memor. Soc. Geol. Ital. 38, 163–176.

Delvaux, D., Sperner, B., 2003. New Aspects of Tectonic Stress Inversion with Reference to the TENSOR Program, vol. 212. Geological Society, London, Special Publications, pp. 75–100. https://doi.org/10.1144/GSL.SP.2003.212.01.06.

Destro, N., 1995. Release fault: a variety of cross fault in linked extensional fault systems, in the Sergipe-Alagoas Basin, NE Brazil. J. Struct. Geol. 17, 615–629. https://doi.org/10.1016/0191-8141(94)00088-H.

Di Bucci, D., Mazzoli, S., 2003. The October–November 2002 Molise seismic sequence (southern Italy): an expression of Adria intraplate deformation. J. Geol. Soc. 160, 503–506. https://doi.org/10.1144/0016-764902-152.

Di Bucci, D., Ravaglia, A., Seno, S., Toscani, G., Fracassi, U., Valensise, G., 2006. Seismotectonics of the southern Apennines and Adriatic foreland: insights on active regional E-W shear zones from analogue modeling. Tectonics 25 (4).

Di Luccio, F., Fukuyama, E., Pino, N.A., 2005. The 2002 Molise earthquake sequence: what can we learn about the tectonics of southern Italy? Tectonophysics 405 (1–4), 141–154.

Doglioni, C., 1991. A proposal for the kinematic modelling of W-dipping subductions-possible applications to the Tyrrhenian-Apennines system. Terra. Nova 3, 423–434.

Dolan, J.F., Haravitch, B.D., 2014. How well do surface slip measurements track slip at depth in large strike-slip earthquakes? The importance of fault structural maturity in controlling on-fault slip versus off-fault surface deformation. Earth Planet Sci. Lett. 388, 38–47. https://doi.org/10.1016/j.epsl.2013.11.043.

Fellin, M.G., San Jose, M., Faccenna, C., Willett, S.D., Cosentino, D., Lanari, R., Gourbet, L., Maden, C., 2021. Transition from slab roll-back to slab break-off in the

central Apennines, Italy: constraints from the stratigraphic and thermochronologic record. GSA Bulletin. https://doi.org/10.1130/B36123.1.
Ferranti, L., Oldow, J.S., 2005. Latest miocene to quaternary horizontal and vertical displacement rates during simultaneous contraction and extension in the Southern Apennines orogen, Italy. Terra Nova 17 (3), 209–214.
Ferrill, D.A., Morris, A.P., McGinnis, R.N., 2012. Extensional fault-propagation folding in mechanically layered rocks: the case against the frictional drag mechanism. Tectonophysics 576, 78–85.
Ferrill, D.A., Morris, A.P., McGinnis, R.N., Smart, K.J., Wigginton, S.S., Hill, N.J., 2017. Mechanical stratigraphy and normal faulting. J. Struct. Geol. 94, 275–302.
Finetti, I., 1982. Structure, stratigraphy and evolution of central Mediterranean. Bollettino Di Geofisica Teorica e Applicata 14, 247–312.
Finetti, I.R., Del Ben, A., 2005a. Crustal tectono-stratigraphic setting of the Adriatic Sea from new CROP seismic data. CROP project. Deep seismic exploration of the Central Mediterranean and Italy 1, 519–548.
Finetti, I.R., Del Ben, A., 2005b. Crustal tectono-stratigraphic setting of the Adriatic Sea from new CROP seismic data. CROP PROJECT. Deep seismic exploration of the Central Mediterranean and Italy 1, 519–548.
Gawthorpe, R.L., Leeder, M.R., 2000. Tectono-sedimentary evolution of active extensional basins. Basin Res. 12, 195–218. https://doi.org/10.1111/j.1365-2117.2000.00121.x.
Ghisetti, F., Vezzani, L., 1997. Interfering paths of deformation and development of arcs in the fold-and-thrust belt of the central Apennines (Italy). Tectonics 16, 523–536.
Guidoboni, E., Ferrari, G., Tarabusi, G., Sgattoni, G., Comastri, A., Mariotti, D., Valensise, G., 2019. CFTI5Med, the new release of the catalogue of strong earthquakes in Italy and in the Mediterranean area. Sci. Data 6 (1), 80.
Hill, K.C., Hayward, A.B., 1988. Structural constraints on the Tertiary plate tectonic evolution of Italy. Mar. Petrol. Geol. 5, 2–16.
ISIDe Working Group, 2007. Italian Seismological Instrumental and Parametric Database (ISIDe).
Kim, Y.-S., Sanderson, D.J., 2006. Structural similarity and variety at the tips in a wide range of strike–slip faults: a review. Terra. Nova 18, 330–344. https://doi.org/10.1111/j.1365-3121.2006.00697.x.
La Bruna, V., Agosta, F., Lamarche, J., Viseur, S., Prosser, G., 2018. Fault growth mechanisms and scaling properties in foreland basin system: the case study of Monte Alpi, Southern Apennines, Italy. J. Struct. Geol. 116, 94–113. https://doi.org/10.1016/j.jsg.2018.08.009.
Lacombe, O., Mouthereau, F., 2002. Basement-involved shortening and deep detachment tectonics in forelands of orogens: insights from recent collision belts (Taiwan, Western Alps, Pyrenees). Tectonics 21. https://doi.org/10.1029/2001TC901018, 12-1-12-22.
Lacombe, O., Malandain, J., Vilasi, N., Amrouch, K., Roure, F., 2009. From paleostresses to paleoburial in fold–thrust belts: preliminary results from calcite twin analysis in the Outer Albanides. Tectonophysics, The Geology of Vertical Movements of the Lithosphere 475, 128–141. https://doi.org/10.1016/j.tecto.2008.10.023.
Lisle, R.J., Srivastava, D.C., 2004. Test of the frictional reactivation theory for faults and validity of fault-slip analysis. Geology 32 (7), 569–572.
Livio, F., Kettermann, M., Reicherter, K., Urai, J.L., 2018. Growth of bending-moment faults due to progressive folding: insights from sandbox models and paleoseismological implications. Geomorphology. https://doi.org/10.1016/j.geomorph.2018.02.012.
Maesano, F.E., D'Ambrogi, C., Burrato, P., Toscani, G., 2015. Slip-rates of blind thrusts in slow deforming areas: examples from the Po Plain (Italy). Tectonophysics 643, 8–25.
Malinverno, A., Ryan, W.B., 1986. Extension in the Tyrrhenian Sea and shortening in the Apennines as result of arc migration driven by sinking of the lithosphere. Tectonics 5, 227–245.
Malusà, M.G., Danišík, M., Kuhlemann, J., 2016. Tracking the adriatic-slab travel beneath the tethyan margin of corsica–sardinia by low-temperature thermochronometry. Gondwana Res. 31, 135–149. https://doi.org/10.1016/j.gr.2014.12.011.
Mancinelli, P., Scisciani, V., 2020. Seismic velocity-depth relation in a siliciclastic turbiditic foreland basin: a case study from the Central Adriatic Sea. Mar. Petrol. Geol. 120, 104554. https://doi.org/10.1016/j.marpetgeo.2020.104554.
Marrett, R., Allmendinger, R.W., 1990. Kinematic analysis of fault-slip data. J. Struct. Geol. 12, 973–986. https://doi.org/10.1016/0191-8141(90)90093-E.
Mazzoli, S., 2000. Time and space variability of thin-skinned and thick-skinned thrust tectonics in the Appennines (Italy). In: Atti Della Accademia Nazionale Dei Lincei. Rendiconti. Classe Di Scienze Fisiche, vol. 11. Matematiche e Naturali.
McGinnis, R.N., Ferrill, D.A., Morris, A.P., Smart, K.J., 2016. Insight on Mechanical Stratigraphy and Subsurface Interpretation.
Merlini, S., Mostardini, F., 1986. Appennino centro-meridionale: Sesioni geologiche e proposta di modello strutturale. Geologia Dell'Italia Centrale. Congresso Nazionale. 73, 147–149.
Mindszenty, A., D'Argenio, B., Aiello, G., 1995. Lithospheric bulges recorded by regional unconformities. The case of Mesozoic-Tertiary Apulia. Tectonophysics 252 (1–4), 137–161.
Morley, C.K., 2002. A tectonic model for the Tertiary evolution of strike–slip faults and rift basins in SE Asia. Tectonophysics 347, 189–215. https://doi.org/10.1016/S0040-1951(02)00061-6.
Morris, A., Ferrill, D.A., Henderson, D.B., 1996. Slip-tendency analysis and fault reactivation. Geology 24 (3), 275–278.
Mouthereau, F., Lacombe, O., 2006. Inversion of the paleogene Chinese continental margin and thick-skinned deformation in the western foreland of taiwan. Journal of Structural Geology, Tectonic Inversion and Structural Inheritance in Mountain Belts 28, 1977–1993. https://doi.org/10.1016/j.jsg.2006.08.007.
Naliboff, J.B., Buiter, S.J.H., Péron-Pinvidic, G., Osmundsen, P.T., Tetreault, J., 2017. Complex fault interaction controls continental rifting. Nat. Commun. 8, 1–9. https://doi.org/10.1038/s41467-017-00904-x.
Naylor, M.A., Mandl, G. t, Supesteijn, C.H.K., 1986. Fault geometries in basement-induced wrench faulting under different initial stress states. J. Struct. Geol. 8, 737–752.
Pace, P., Calamita, F., 2014. Push-up inversion structures v. fault-bend reactivation anticlines along oblique thrust ramps: examples from the Apennines fold-and-thrust belt (Italy). J. Geol. Soc. 171, 227–238. https://doi.org/10.1144/jgs2013-053.
Pace, P., Scisciani, V., Calamita, F., Butler, R.W.H., Iacopini, D., Esestime, P., Hodgson, N., 2015. Inversion structures in a foreland domain: seismic examples from the Italian Adriatic Sea. Interpretation 3 (1), SAA161–SAA176. https://doi.org/10.1190/INT-2015-0013.
Patacca, E., Scandone, P., 1989. Post-Tortonian mountain building in the Apennines. The role of the passive sinking of a relic lithospheric slab. Atti dei Convegni Lincei 80, 157–176.
Patacca, E., Scandone, P., 2007. Geology of the southern Apennines. Boll. Soc. Geol. Ital. 7, 75–119.
Patacca, E., Scandone, P., Crescenti, U., 2004. The Plio-Pleistocene thrust belt-foredeep system in the southern Apennines and Sicily (Italy). Geology of Italy 32, 93–129.
Patacca, E., Scandone, P., Di Luzio, E., Cavinato, G.P., Parotto, M., 2008. Structural architecture of the central Apennines: interpretation of the CROP 11 seismic profile from the Adriatic coast to the orographic divide. Tectonics 27.
Phillips, T.B., Jackson, C.A.-L., Bell, R.E., Duffy, O.B., Fossen, H., 2016. Reactivation of intrabasement structures during rifting: a case study from offshore southern Norway. J. Struct. Geol. 91, 54–73. https://doi.org/10.1016/j.jsg.2016.08.008.
Piana Agostinetti, N., Faccenna, C., 2018. Deep structure of Northern Apennines subduction orogen (Italy) as revealed by a joint interpretation of passive and active seismic data. Geophys. Res. Lett. 45, 4017–4024.
Piccardi, L., Sani, F., Moratti, G., Cunningham, D., Vittori, E., 2011. Present-day geodynamics of the circum-Adriatic region: an overview. J. Geodyn. 51, 81–89.
Quintà, A., Tavani, S., 2012. The foreland deformation in the south-western Basque–Cantabrian Belt (Spain). Tectonophysics, Into the Deformation History of Folded Rocks 576–577, 4–19. https://doi.org/10.1016/j.tecto.2012.02.015.
Ricchetti, G., Ciaranfi, N., Luperto Sinni, E., Mongelli, F., Pieri, P., 1988. Geodinamica ed evoluzione sedimentaria e tettonica dell'avampaese apulo. Memor. Soc. Geol. Ital. 41, 57–82.
Roche, V., Homberg, C., Rocher, M., 2012. Fault displacement profiles in multilayer systems: from fault restriction to fault propagation: evolution of the fault displacement profile. Terra. Nova 24, 499–504. https://doi.org/10.1111/j.1365-3121.2012.01088.x.
Rotevatn, A., Jackson, C.A.-L., Tvedt, A.B.M., Bell, R.E., Blækkan, I., 2018. How do normal faults grow? J. Struct. Geol. https://doi.org/10.1016/j.jsg.2018.08.005.
Rovida, A.N., Locati, M., Camassi, R.D., Lolli, B., Gasperini, P., 2016. CPTI15, the 2015 Version of the Parametric Catalogue of Italian Earthquakes.
Rovida, A.N., Locati, M., Camassi, R.D., Lolli, B., Gasperini, P., 2019. Catalogo parametrico dei terremoti italiani cpti15, versione 2.0.Chicago.
Royden, L., Faccenna, C., 2018. Subduction orogeny and the late cenozoic evolution of the mediterranean arcs. Annu. Rev. Earth Planet Sci. 46, 261–289.
Royden, L., Patacca, E., Scandone, P., 1987. Segmentation and configuration of subducted lithosphere in Italy: an important control on thrust-belt and foredeep-basin evolution. Geology 15, 714–717.
Sabbatino, M., Tavani, S., Vitale, S., Ogata, K., Corradetti, A., Consorti, L., Arienzo, I., Cipriani, A., Parente, M., 2021. Forebulge migration in the foreland basin system of the central-southern Apennine fold-thrust belt (Italy): new high-resolution Sr-isotope dating constraints. Basin Res. 33, 2817–2836. https://doi.org/10.1111/bre.12587.
Santantonio, M., Scrocca, D., Lipparini, L., 2013. The ombrina-rospo plateau (apulian platform): evolution of a carbonate platform and its margins during the jurassic and cretaceous. Mar. Petrol. Geol. 42, 4–29.
Scisciani, V., 2009. Styles of positive inversion tectonics in the Central Apennines and in the Adriatic foreland: implications for the evolution of the Apennine chain (Italy). J. Struct. Geol. 31, 1276–1294. https://doi.org/10.1016/j.jsg.2009.02.004.
Scisciani, V., Calamita, F., 2009. Active intraplate deformation within Adria: examples from the adriatic region. Tectonophysics, Ten Years after the Umbria-Marche Earthquake, Central Italy 476, 57–72. https://doi.org/10.1016/j.tecto.2008.10.030.
Scisciani, V., Esestime, P., 2017. Chapter 23 - the triassic evaporites in the evolution of the adriatic basin. In: Soto, J.I., Flinch, J.F., Tari, G. (Eds.), Permo-Triassic Salt Provinces of Europe, North Africa and the Atlantic Margins. Elsevier, pp. 499–516. https://doi.org/10.1016/B978-0-12-809417-4.00024-0.
Scisciani, V., Montefalcone, R., 2006. Coexistence of Thin-And Thick-Skinned Tectonics: an Example from the Central Apennines. Italy.
Scrocca, D., 2006. Thrust front segmentation induced by differential slab retreat in the Apennines (Italy). Terra. Nova 18, 154–161. https://doi.org/10.1111/j.1365-3121.2006.00675.x.
Scrocca, D., Carminati, E., Doglioni, C., 2005. Deep structure of the southern Apennines, Italy: thin-skinned or thick-skinned? Tectonics 24.
Segall, P., Pollard, D.D., 1980. Mechanics of discontinuous faults. J. Geophys. Res. Solid Earth 85, 4337–4350. https://doi.org/10.1029/JB085iB08p04337.
Shiner, P., Beccacini, A., Mazzoli, S., 2004a. Thin-skinned versus thick-skinned structural models for Apulian carbonate reservoirs: constraints from the Val d'Agri Fields, S Apennines, Italy. Mar. Petrol. Geol. 21 (7), 805–827.
Shiner, P., Beccacini, A., Mazzoli, S., 2004b. Thin-skinned versus thick-skinned structural models for Apulian carbonate reservoirs: constraints from the Val d'Agri Fields, S Apennines, Italy. Mar. Petrol. Geol. 21, 805–827. https://doi.org/10.1016/j.marpetgeo.2003.11.020.

Soliva, R., Benedicto, A., 2005. Geometry, scaling relations and spacing of vertically restricted normal faults. J. Struct. Geol. 27, 317–325. https://doi.org/10.1016/j.jsg.2004.08.010.

Soliva, R., Benedicto, A., Maerten, L., 2006. Spacing and linkage of confined normal faults: importance of mechanical thickness. J. Geophys. Res. Solid Earth 111. https://doi.org/10.1029/2004JB003507.

Sylvester, A.G., 1988. Strike-slip faults. GSA Bulletin 100 (2), 1666–1703. https://doi.org/10.1130/0016-7606(1988)100<1666:SSF>2.3.CO.

Tavani, S., Storti, F., Salvini, F., 2006. Double-edge fault-propagation folding: geometry and kinematics. J. Struct. Geol. 28, 19–35. https://doi.org/10.1016/j.jsg.2005.09.007.

Tavani, S., Storti, F., Lacombe, O., Corradetti, A., Muñoz, J.A., Mazzoli, S., 2015a. A review of deformation pattern templates in foreland basin systems and fold-and-thrust belts: implications for the state of stress in the frontal regions of thrust wedges. Earth Sci. Rev. 141, 82–104. https://doi.org/10.1016/j.earscirev.2014.11.013.

Tavani, S., Vignaroli, G., Parente, M., 2015b. Transverse versus longitudinal extension in the foredeep-peripheral bulge system: role of Cretaceous structural inheritances during early Miocene extensional faulting in inner central Apennines belt. Tectonics 34, 1412–1430. https://doi.org/10.1002/2015TC003836.

Tavani, S., Granado, P., Corradetti, A., Camanni, G., Vignaroli, G., Manatschal, G., Mazzoli, S., Muñoz, J.A., Parente, M., 2021. Rift inheritance controls the switch from thin- to thick-skinned thrusting and basal décollement re-localization at the subduction-to-collision transition. GSA Bulletin 133, 2157–2170. https://doi.org/10.1130/B35800.1.

Tondi, E., Piccardi, L., Cacon, S., Kontny, B., Cello, G., 2005. Structural and time constraints for dextral shear along the seismogenic Mattinata Fault (Gargano, southern Italy). J. Geodyn. 40, 134–152. https://doi.org/10.1016/j.jog.2005.07.003.

Turcotte, D.L., Schubert, G., 2002. Geodynamics. Cambridge University Press.

Tvedt, A.B.M., Rotevatn, A., Jackson, C.A.-L., Fossen, H., Gawthorpe, R.L., 2013. Growth of normal faults in multilayer sequences: a 3D seismic case study from the Egersund Basin, Norwegian North Sea. J. Struct. Geol. 55, 1–20. https://doi.org/10.1016/j.jsg.2013.08.002.

Vai, F., Martini, I.P., 2013. Anatomy of an Orogen: the Apennines and Adjacent Mediterranean Basins. Springer.

van Gent, H.W., Holland, M., Urai, J.L., Loosveld, R., 2010. Evolution of fault zones in carbonates with mechanical stratigraphy–Insights from scale models using layered cohesive powder. J. Struct. Geol. 32 (9), 1375–1391.

Vitale, S., Ciarcia, S., 2013. Tectono-stratigraphic and kinematic evolution of the southern Apennines/Calabria–Peloritani Terrane system (Italy). Tectonophysics 583, 164–182.

Vlahović, I., Tišljar, J., Velić, I., Matičec, D., 2005. Evolution of the adriatic carbonate platform: palaeogeography, main events and depositional dynamics. Palaeogeogr. Palaeoclimatol. Palaeoecol. 220, 333–360.

Wilkins, S.J., Gross, M.R., 2002. Normal fault growth in layered rocks at Split Mountain, Utah: influence of mechanical stratigraphy on dip linkage, fault restriction and fault scaling. J. Struct. Geol. 24, 1413–1429. https://doi.org/10.1016/S0191-8141(01)00154-7.

Winter, T., Tapponnier, P., 1991. Extension majeure post-Jurassique et ante-Miocene dans le centre de l'Italie; donnees microtectoniques. Bull. Soc. Geol. Fr. 162, 1095–1108.

Ziegler, P.A., Cloetingh, S., van Wees, J.-D., 1995a. Dynamics of intra-plate compressional deformation: the Alpine foreland and other examples. Tectonophysics 252, 7–59. https://doi.org/10.1016/0040-1951(95)00102-6.

Ziegler, P.A., Cloetingh, S., van Wees, J.-D., 1995b. Dynamics of intra-plate compressional deformation: the Alpine foreland and other examples. Tectonophysics 252, 7–59.